

1 **TbasCO: Trait-based Comparative 'Omics Identifies Ecosystem-Level and Niche-  
2 Differentiating Adaptations of an Engineered Microbiome**

3  
4 McDaniel, E.A.<sup>1,2#\*</sup>, van Steenbrugge, J.J.M<sup>3,4,5#+</sup>, Noguera, D.R.<sup>6</sup>, McMahon, K.D.<sup>1,6</sup>,  
5 Raaijmakers, J.M.<sup>4,7</sup>, Medema, M.H.<sup>3,7</sup>, Oyserman, B.O.<sup>3,4+</sup>  
6  
7

8 <sup>1</sup> Department of Bacteriology, University of Wisconsin – Madison, Madison, WI, USA

9 <sup>2</sup> Microbiology Doctoral Training Program, University of Wisconsin - Madison, Madison, WI, USA

10 <sup>3</sup> Bioinformatics Group, Wageningen University and Research, Wageningen, The Netherlands

11 <sup>4</sup> Microbial Ecology, Netherlands Institute of Ecological Research, Wageningen, The  
12 Netherlands

13 <sup>5</sup> Laboratory of Nematology, Wageningen University, Wageningen, The Netherlands

14 <sup>6</sup> Department of Civil and Environmental Engineering, University of Wisconsin – Madison,  
15 Madison WI USA

16 <sup>7</sup> Institute of Biology, Leiden University, Leiden, Netherlands

17 <sup>#</sup> = contributed equally

18 <sup>+</sup> = corresponding author

19

20 \* Current address:

21 Department of Microbiology and Immunology, University of British Columbia, Vancouver, CA

22

23 Corresponding authors:

24 Elizabeth McDaniel [elizabethmcd93@gmail.com](mailto:elizabethmcd93@gmail.com)

25 Joris van Steenbrugge [jorisvansteebrugge@gmail.com](mailto:jorisvansteebrugge@gmail.com)

26 Ben Oyserman [BenOyserman@gmail.com](mailto:BenOyserman@gmail.com)

27

28

29 **ABSTRACT**

30 A grand challenge in microbial ecology is disentangling the traits of individual  
31 populations within complex communities. Various cultivation-independent approaches  
32 have been used to infer traits based on the presence of marker genes. However, marker  
33 genes are not linked to traits with complete fidelity, nor do they capture important  
34 attributes, such as the timing of expression or coordination among traits. To address this,  
35 we present an approach for assessing the trait landscape of microbial communities by  
36 statistically defining a trait attribute as shared transcriptional pattern across multiple  
37 organisms. Leveraging the KEGG pathway database as a trait library and the Enhanced  
38 Biological Phosphorus Removal (EBPR) model microbial ecosystem, we demonstrate  
39 that a majority (65%) of traits present in 10 or more genomes have niche-differentiating  
40 expression attributes. For example, while 14 genomes containing the high-affinity  
41 phosphorus transporter *pstABCS* display a canonical attribute (e.g. up-regulation under  
42 phosphorus starvation), we identified another attribute shared by 11 genomes where  
43 transcription was highest under high phosphorus conditions. Taken together, we provide  
44 a novel framework for revealing hidden metabolic versatility when investigating genomic  
45 data alone by assigning trait-attributes through genome-resolved time-series  
46 metatranscriptomics.

47

48

49

50

51

## 52 INTRODUCTION

53 A longstanding cornerstone of deterministic ecological theory is that the  
54 environment selects for traits. Traits may be defined as any physiological, morphological,  
55 or genomic signature that affects the fitness or function of an individual [1]. Trait-based  
56 approaches have become indispensable in macroecological systems to describe fitness  
57 trade-offs and the effects of biodiversity on ecosystem functioning [2–5]. Recently, trait-  
58 based frameworks have been proposed as an alternative to taxonomy-based methods  
59 for describing microbial ecosystem processes [6, 7]. Connecting microbial traits and their  
60 phylogenetic distributions to ecosystem performance can provide powerful insights into  
61 the ecological and evolutionary dynamics underpinning community assembly, microbial  
62 biogeography, and organismal responses to changes in the environment [8–10].  
63 Additionally, pinpointing the organismal distribution of traits and the selective pressures  
64 that enrich them may be leveraged to reproducibly and rationally engineer stable,  
65 functionally redundant ecosystems [11–15]. However, applying trait-based approaches to  
66 microbial communities is challenging due to the difficulty in identifying and measuring  
67 relevant ecological traits for a given ecosystem [16].

68 High-throughput sequencing technologies and multi-omics techniques have been  
69 used to describe the diversity, activity, and functional potential of uncultivated microbial  
70 lineages [17–20]. Improvements in bioinformatics algorithms, and in particular  
71 metagenomic binning methods, have allowed for genome-resolved investigations of  
72 microbial communities rather than gene-based analyses of assembled contigs [21].  
73 These (meta) genomes are subsequently leveraged to detect the presence of key genes  
74 or pathways and predict specific traits of the whole community [22, 23]. Integrating

75 metatranscriptomics data addresses a key limitation, as expression patterns better reflect  
76 the actual functional dynamics of a trait compared to gene presence alone. Here, we  
77 present TbasCO, a software package and statistical framework for *Trait-based*  
78 Comparative ‘Omics to identify expression attributes. We adopt the terminology *attribute*  
79 as a hierarchically structured feature of a trait and assert that statistically similar  
80 transcriptional patterns of traits across multiple organisms be treated as *attributes* (Figure  
81 1). In this manner, the identification of expression-based *attributes* provides a high-  
82 throughput and intuitive framework for extending trait-based methods to time-series  
83 expression patterns in microbial communities. We implement this trait-based approach to  
84 classify transcriptional attributes in a microbial community performing Enhanced  
85 Biological Phosphorus Removal (EBPR), a globally important biotechnological process  
86 implemented in numerous wastewater treatment plants (WWTPs).

87 The fundamental feature of the engineered EBPR ecosystem is the decoupled and  
88 cyclic availability of an external carbon source and terminal electron acceptor. This cycling  
89 is often referred to as “feast-famine” conditions and provides a strong selective pressure  
90 for traits such as polymer cycling. Accumulation of intracellular polyphosphate through  
91 cyclic anaerobic-aerobic conditions ultimately results in net phosphorus removal and  
92 accomplishes the EBPR process [24, 25]. One of the most well-studied polyphosphate  
93 accumulating organisms (PAOs) belongs to the uncultivated bacterial lineage  
94 ‘*Candidatus Accumulibacter phosphatis*’ (hereby referred to as *Accumulibacter*) [24, 26].  
95 Numerous genome-resolved ‘omics methods have been used to investigate the  
96 physiology and regulation of this model PAO enriched in engineered lab-scale enrichment  
97 bioreactor systems [27–34]. However, novel and putative PAOs have been discovered

98 that remove phosphorus without exhibiting the hallmark traits of *Accumulibacter* [35–39].  
99 Additionally, although these lab-scale systems are designed to specifically enrich for  
100 *Accumulibacter*, a diverse “flanking community” persists in these environments [27], and  
101 their ecological roles have largely remained unexplored. As a result, the general  
102 adaptations of microbial lineages inhabiting the EBPR community are not well  
103 understood. Using genome-resolved metagenomics and metatranscriptomics, we  
104 assembled 66 species-representative genomes spanning several significant EBPR  
105 lineages and identified the distribution of expression-based attributes. Using our novel  
106 trait-based comparative ‘omics approach, we show that while some expression attributes  
107 are distributed in few genomes, many are redundant and shared across many lineages.  
108 Furthermore, we find that a majority of core traits (as defined by the presence of marker  
109 genes) have multiple attributes, suggesting that identifying niche-differentiating  
110 expression attributes may be used to reveal a large hidden metabolic versatility when  
111 investigating genomic data alone.

112

## 113 MATERIALS AND METHODS

### 114 Metagenomic Assembly, Annotation, and Metatranscriptomic Mapping

115 Three metagenomes sampled from an EBPR bioreactor with linked time-series  
116 metatranscriptomics data [40] were collected for metagenomic sequencing and  
117 assembled into 66 species-representative bins as described in the Supplemental  
118 Methods. All bins are greater than 75% complete and contain less than 10%  
119 contamination, with a large majority (44/66) >95% complete and <5% redundant as  
120 calculated by CheckM [41] (Table 1). Each bin was functionally annotated using the

121 KEGG database through an HMM-based approach under KEGG release 93.0 using the  
122 command-line KofamKOALA pipeline [42, 43], selecting annotations that were significant  
123 hits above the specific HMM threshold. This resulted in 117,657 total annotations with  
124 5,228 unique annotations. We used a metatranscriptomic dataset of six timepoints  
125 collected over a single EBPR cycle from Oyserman et al. 2016 [40], with three timepoints  
126 from the anaerobic phase and three from the aerobic phase. Raw reads were quality  
127 filtered using BBtools suite v38.07 [44] and ribosomal rRNA was removed from each  
128 sample using SortMeRNA [45]. Reads from each sample were mapped against the  
129 concatenated set of open reading frames from all 66 bins using kallisto v0.44.0 and  
130 parsed using the R package tximport [46, 47].

131 **TbasCO Method Implementation**

132 The TbasCO package identifies expression-based attributes of predefined traits  
133 using time-series (meta)transcriptomics data (Figure 1). In general, traits are defined by  
134 the presence of a pathway or other collection of genes from an externally provided  
135 database. A weighted distance metric between expression patterns for all genes that  
136 define a trait is calculated, and statistically significant similarity is determined based on  
137 the background distribution of a trait of equal size. Thereby, two or more organisms with  
138 a statistically similar expression pattern for a trait share an *attribute*.

139 ***Input and Preprocessing***

140 The input that is accepted by TbasCO is a table of RNAseq counts in csv format.  
141 Each row is treated as gene that has columns for the gene/locus name, counts per  
142 sample, the genome the gene belongs to, and the KEGG Orthology (KO) identifier. The  
143 RNAseq counts table may be provided pre-normalized or can be normalized by the

144 program. The default normalization method is designed to minimize compositional bias in  
145 the differential abundance and activity of constituent populations in metatranscriptomics  
146 studies. Raw RNA expression counts are therefore normalized by genomic bin and  
147 sample [40]. These normalization factors are then applied to each sample for each bin  
148 individually. Alternatively, custom normalization methods may be implemented. After  
149 normalization, a pruning step is introduced to filter genes that have zero counts or a mean  
150 absolute deviation of less than one. To make inter-organismal comparisons of the relative  
151 contribution of a gene to total measured organismal RNA, an additional statistic is  
152 calculated ranking the expression counts from each sample from highest to lowest. The  
153 ranks for each sample are then normalized by dividing them by the maximum rank value  
154 in that sample. This normalization is applied to make ranks comparable between  
155 organisms with different genome sizes.

156 To assess the statistical significance of the calculated distances between the  
157 expression patterns of all genes within a trait, random background distributions are  
158 created for 1) individual genes and 2) traits of N genes. For individual genes, three  
159 different distributions were calculated, based on the distances between randomly  
160 sampled open reading frames, randomly sampled genes with an annotation (but not  
161 necessarily the same annotation), and randomly sampled genes with the same  
162 annotation. The background distribution for a trait of N genes is based on the distances  
163 between randomly composed sets of genes. For each gene pair, two distances metrics  
164 are calculated, the Pearson Correlation (PC) and the Normalized Rank Euclidean  
165 Distance (NRED). In practice, it is often found that a certain annotation is assigned to  
166 multiple genes in the same genome. If this occurs, there is an option to use either a

167 random selection, or the highest scoring pair. In the latter case, a correction for multiple  
168 testing is implemented. This process is repeated N-times, where N equals the number of  
169 genes in any given trait. The background distribution for traits is determined by first  
170 randomly sampling two genomes, identifying the overlap in annotations, and finally  
171 artificially defining a trait containing N annotations. For each annotation in the trait, the  
172 distances are calculated between genome A and genome B, as described in the previous  
173 section. As modules vary in size, this process is repeated for traits of different sizes.

174 ***Identifying Attributes***

175 TbasCO provides both a cluster-based and pair-wise approach to identify  
176 attributes. In both methods, the distance between expression patterns of a trait between  
177 two genomes is first calculated based on a composite Z score of the PC and NRED for  
178 each gene composing the trait. In the cluster-based analysis, the distances are  
179 subsequently clustered using the Louvain clustering algorithm to identify trait attributes.  
180 To determine if an attribute is significantly similar or not, a one-sided T-test between the  
181 attribute and the random background distribution of traits is conducted. This is done for  
182 both cluster-based and model-based comparisons. Many traits are complex and  
183 represented in databases such as KEGG by numerous alternative routes. To deal with  
184 this complexity, each pathway is expanded into the Disjunctive Normative Form (DNF).  
185 Due to the extremely high number of DNFs for some traits, attributes are pruned based  
186 on a strict requirement of 100% completion.

187 ***Distance Calculations***

188 To determine the similarity in expression patterns between genes, two distance  
189 metrics are calculated: the PC between RNAseq counts across samples, and the NRED,

190 where ranks are a measure of relative abundance of RNA in each sample, normalized  
191 the abundance of RNA in the corresponding genome. These distance scores are  
192 converted to Z scores using a background distribution of distances between randomly  
193 sampled genes as previously described. To determine statistically significant similarities  
194 between the expression patterns of a trait between two genomes, a composite distance  
195 score is calculated based on the distance between genes in two different genomes. For  
196 each of these genes the PC and NRED are calculated and transformed to Z scores and  
197 combined as  $(-1*PC + NRED)$ . The distance of the trait between two genomes is defined  
198 as the average of these composite distance scores, and then normalized by the Jaccard  
199 distance between these genomes.

200 
$$(-PC + NRED) * (1 - dJ)$$

201 ***Statistical Assessment of Trait Attributes***

202 In both model-based and pair-wise approaches, the distance is first calculated  
203 between expression patterns of a trait between two genomes based on the composite Z  
204 score of the PC and NRED for each gene composing the trait. In the clustering-based  
205 analysis, the distances are subsequently clustered using the Louvain clustering algorithm  
206 to identify trait-attributes. To determine if attributes are significantly similar, a one-sided  
207 T-test is conducted between the attribute and a background distribution of randomly  
208 sampled traits with the same number of genes. To derive the random background  
209 distributions, multiple distributions are calculated ranging in gene numbers from the  
210 smallest trait to the largest trait in the dataset as described previously. For each  
211 background distribution, N (default: 10,000) traits are randomly composed. The distances  
212 between these artificial traits are calculated in the same way as for the actual traits. In

213 addition to a statistical pruning step, the attributes are pruned based on a strict  
214 requirement of 100% completion of each DNF module. A benchmarking analysis to  
215 examine the effects of different parameters was conducted to determine their influence  
216 on the number of attributes identified and may be found in the supplementary materials  
217 (Supplementary Table 1, Supplementary Figures 2-4).

218 **Data and Code Availability**

219 All supplementary files and figures including functional annotations and  
220 transcriptome count files are available at [https://figshare.com/projects/EBPR\\_Trait-Based\\_Comparative\\_Omics/90437](https://figshare.com/projects/EBPR_Trait-Based_Comparative_Omics/90437). All 64 flanking genomes have been deposited in  
221 NCBI at Bioproject [PRJNA714686](https://www.ncbi.nlm.nih.gov/bioproject/PRJNA714686). The remaining two reassembled Accumulibacter  
222 genomes have not been deposited in NCBI to not confuse between the original CAPIA  
223 and CAPIIA assemblies [27, 28]. These contemporary assemblies are available at the  
224 Figshare repository. The three metagenomes and six metatranscriptomes used in this  
225 study are available on the JGI/IMG at accession codes 3300026302, 3300026286,  
226 3300009517, and 3300002341-46, respectively. All code for performing metagenomic  
227 assembly, binning, and annotation can be found at  
228 <https://github.com/elizabethmcd/EBPR-MAGs>. The TbasCO method has been  
229 implemented as a reproducible R package and can be accessed at  
230 <https://github.com/Jorisvansteenbrugge/TbasCO>.

232

233

234

235

236 **RESULTS AND DISCUSSION**

237 **Reconstructing a Diverse EBPR SBR Community**

238 To explore trait-based transcriptional dynamics of a semi-complex microbial  
239 community, we applied genome-resolved metagenomics and metatranscriptomics to an  
240 EBPR sequencing-batch reactor (SBR) ecosystem (Figure 2). We previously performed  
241 a metatranscriptomics time-series experiment over the course of a normally operating  
242 EBPR cycle to investigate the regulatory controls of *Accumulibacter* gene expression [40].  
243 In this experiment, six samples were collected for RNA sequencing: three from the  
244 anaerobic phase and three from the aerobic phase (Figure 2A). Additionally, three  
245 metagenomes were collected from the same month of the metatranscriptomic  
246 experiment, including a sample from the same date of the experiment. We reassembled  
247 contemporary *Accumulibacter* clade IIA and IA genomes that were previously assembled  
248 from the same bioreactor system [27, 28]. The genomes of *Accumulibacter* clades IA and  
249 IIA are similar by approximately 85% average-nucleotide identity [28], and although this  
250 is well below the common species-resolved cutoff of 95% [48], we refer to the clade  
251 nomenclature defined based on polyphosphate kinase (*ppk1*) sequence identity [49, 50].  
252 During the experiment, the bioreactor was highly enriched in *Accumulibacter* clade IIA,  
253 accounting for approximately 50% of the mapped metagenomic reads and the highest  
254 transcriptional counts (Figures 2B and 2C) [40]. Whereas *Accumulibacter* clade IA  
255 exhibited low abundance patterns but was within the top 10 genomes with the highest  
256 total transcriptional counts (Figure 2C).

257 Although this bioreactor system was highly enriched in *Accumulibacter*, a diverse  
258 flanking community persisted and was active in this ecosystem (Figure 2B, C). We

259 reconstructed representative population genomes of the microbial community of the SBR  
260 system, resulting in 64 metagenome-assembled genomes (MAGs) of the flanking  
261 community. Interestingly, we recovered genomes of experimentally verified and putative  
262 PAOs, including two *Tetrasphaera* spp. (TET1 and TET2) ‘*Candidatus Obscuribacter*  
263 *phosphatis*’ (OBS1), and *Gemmatimonadetes* (GEMMA1). Pure cultures of *Tetrasphaera*  
264 have been experimentally shown to cycle polyphosphate without incorporating PHA [36],  
265 deviating from the hallmark Accumulibacter PAO model. The first cultured representative  
266 of the *Gemmatimonadetes* phylum *Gemmatimonas aurantiaca* was isolated from an SBR  
267 simulating EBPR and was shown to accumulate polyphosphate through Neisser and  
268 DAPI staining [51]. Additionally, *Ca. Obscuribacter phosphatis* has been hypothesized to  
269 cycle phosphorus based on the presence of genes for phosphorus transport,  
270 polyphosphate incorporation, and potential for both anaerobic and aerobic respiration  
271 [37], and has also been enriched in photobioreactor EBPR systems [52]. Both  
272 *Tetrasphaera* spp. TET1 and TET2, OBS1, and GEMMA1 groups exhibit higher relative  
273 abundance patterns than CAPIA but have similar relative transcriptional levels (Figure 2B  
274 and 2C, Table 1).

275 Numerous SBR MAGs among the *Actinobacteria* and *Proteobacteria* contain the  
276 metabolic potential for phosphorus cycling based on the presence of the high-affinity  
277 phosphorus transporter *pstABCS* system, polyphosphate kinase *ppk1*, and the low-  
278 affinity *pit* phosphorus transporter (Supplementary Figure 5). Additionally, select MAGs  
279 within the *Alphaproteobacteria*, *Betaproteobacteria*, and *Gammaproteobacteria* contain  
280 all required subunits for polyhydroxyalkanoate synthesis (Supplementary Figure 5). Other  
281 abundant and transcriptionally active groups in the SBR ecosystem that are not predicted

282 to be PAOs are members of the *Bacteroidetes* such as CHIT1 within the  
283 *Chitinophagaceae*, and *Cytophagales* members *Runella* sp. RUN1 and *Leadbetterella* sp.  
284 LEAD1 (Figure 2B and 2C, Table 1). Interestingly, an uncharacterized group within the  
285 *Bacteroidetes* BAC1 contributed the third most to the pool of transcripts (Figure 2C), and  
286 did not show phylogenetic similarity to MAGs assembled from Danish full-scale  
287 wastewater treatment systems [39] (Supplementary Figure 1). Other groups from which  
288 we assembled MAGs for that do not exhibit clear roles in EBPR systems were *Chloroflexi*  
289 ANAER1 and HERP1 MAGs, *Armatimonadetes* FIMBRI1, *Firmicutes* FUS1, and  
290 *Patescibacteria* SACCH1. Members of the *Chloroflexi* are filamentous bacteria that have  
291 been associated with bulking and foaming events in full-scale WWTPS [53–55], but also  
292 aid in forming the scaffolding around floc aggregates and degrade complex polymers [55–  
293 57]. The *Patescibacteria* (formerly TM7) are widespread but low abundant members of  
294 natural and engineered ecosystems, contain reduced genome sizes, and may contribute  
295 to filamentous bulking in activated sludge [21, 58]. To summarize, lab-scale SBRs  
296 designed to enrich for *Accumulibacter* contain diverse flanking community members [27,  
297 32], but their ecological functions and putative interactions remain to be fully understood  
298 in the context of the EBPR ecosystem.

299 **Identifying Expression-Based Trait Attributes Among the EBPR SBR Community  
300 with TbasCO**

301 Current metatranscriptomics approaches often employ either a gene-centric [31,  
302 59–61] or genome-centric approaches [40, 62–64]. In both approaches, highly,  
303 differentially, or co-expressed genes are identified and tested for enrichment of specific  
304 functions. Enrichment- or annotation-based approaches are employed in numerous

305 metatranscriptomics tools such as MG-RAST, MetaTrans, SAMSA2, COMAN, IMP, and  
306 Anvi'o [65–70]. Here, we expand on the use of molecular markers as traits by defining  
307 expression attributes by leveraging *a priori* knowledge from predefined trait libraries, such  
308 as the KEGG database [71], to statistically assess inter-species expression patterns of  
309 genes that together form a trait (Figure 1). First, our results showed that there is  
310 statistically significant transcriptional conservation of genes at the community level; genes  
311 that share an annotation were significantly more similar than expected using two different  
312 distance metrics (NRED: p-value < 2.2e-16, PC: p-value < 2.2e-16). Extending this  
313 statistical analysis to the trait level, we identified 1674 attributes distributed across the 66  
314 genomes. On average, we identified 9.12 genomes per attribute (SD - 5.22), with a  
315 minimum of 3 genomes and a maximum of 35 (Figure 3A). Based on these statistics, we  
316 defined redundant attributes as those two standard deviations above the mean (19  
317 genomes). With this cutoff applied, we identified 79 redundant trait attributes mostly  
318 belonging to pathways among carbohydrate metabolism, purine metabolism, and fatty  
319 acid metabolism categories (Table 2). Of 290 traits, we identified 97 traits with two or  
320 more attributes identified (33%). Of these, traits in 10 or more genomes were twice as  
321 likely to have two or more attributes (65%), suggesting that divergent expression patterns  
322 for a trait are common, and may represent a niche-differentiating feature (Figure 3A).  
323 Henceforth, when multiple attributes are identified for a trait, we refer to these as niche-  
324 differentiating attributes.

325 From the ecosystem perspective, a clear phylogenetic signal is observed in the  
326 distribution of attributes, as genomes cluster together by shared trait attributes by phylum  
327 with some exceptions, such as genomes belonging to the *Bacteroidetes*, *Actinobacteria*,

328 and *Proteobacteria* clustering together, respectively (Figure 3B). For simplicity, we filtered  
329 the network to only include nodes with more than 5 connections. Highly redundant trait  
330 attributes belonged to modules in the lipid metabolism, energy metabolism, and  
331 nucleotide metabolism KEGG functional categories. In contrast, more specialized trait  
332 attributes on the periphery of the network or amongst group-specific clusters such as  
333 within the *Actinobacteria* or subsets of the *Proteobacteria* belonged to amino acid  
334 metabolism, biosynthesis of terpenoids and polyketides, metabolism of cofactors and  
335 vitamins, and carbohydrate metabolism KEGG modules. Pathways of note that showed  
336 a high level of redundancy include the TCA cycle, isoleucine biosynthesis, acyl-CoA  
337 synthesis, threonine biosynthesis, and cytochrome c oxidase activity (Table 2). Large  
338 pathways with hundreds of possible routes such as glycolysis, the TCA cycle,  
339 gluconeogenesis, and the pentose phosphate pathway are not included in the main  
340 network and are displayed as individual networks (Supplementary Figure 6).

341 We next explored the distribution of non-redundant attributes (e.g. 3-18 genomes)  
342 (Figure 3A). A total of 796 trait attributes with low redundancy were identified belonging  
343 to pathways involved in carbohydrate cofactor and vitamin metabolism including  
344 glycolysis, gluconeogenesis, parts of the TCA cycle, tetrahydrofolate biosynthesis,  
345 tryptophan biosynthesis, and the pentose phosphate pathway (Table 3). Different sets of  
346 low redundancy trait attributes were identified within respective phyla (Supplementary  
347 Figure 7). Between genomes belonging to the *Actinobacteria*, *Alphaproteobacteria*,  
348 *Bacteroidetes*, *Betaproteobacteria*, and *Gammaproteobacteria*, low redundancy  
349 attributes (belonging to less than half of the total genomes within the phylum) include  
350 carbohydrate metabolism, amino acid metabolism and metabolism of cofactors and

351 vitamins (Supplementary Figure 7). Redundant trait attributes within individual phyla  
352 belong to core energy metabolism pathways, fatty acid biosynthesis, and carbohydrate  
353 metabolism. However, even within individual phyla, non-redundant attributes include  
354 different amino acids and cofactors (Extended Table 1 - available on Figshare  
355 [https://figshare.com/articles/dataset/Lineage-Specific\\_Core\\_and\\_Niche\\_Differentiating\\_Traits/15001200](https://figshare.com/articles/dataset/Lineage-Specific_Core_and_Niche_Differentiating_Traits/15001200)).

357 As noted previously, one of the most striking findings is that a majority, 65% of  
358 traits present in 10 or more genomes have multiple expression attributes. Thus, it seems  
359 that while the presence of marker genes suggests many organisms share a particular  
360 trait, the presence of niche-differentiating expression profiles suggest an alternative story,  
361 that there is a level of hidden metabolic diversity. For example, central carbon metabolism  
362 and energy pathways such as the TCA cycle, glycolysis, gluconeogenesis, and the  
363 pentose phosphate pathway are oftentimes considered core traits when only analyzing  
364 the presence and/or absence of individual markers belonging to these pathways. Among  
365 over 1000 high-quality MAGs assembled from full-scale Danish WWTPs, the TCA cycle  
366 and pentose phosphate pathway are highly represented among the abundant  
367 microorganisms, with glycolysis less so [39]. Whereas the TCA cycle and pentose  
368 phosphate pathway are present among a high number of genomes in the EBPR SBR  
369 community, different routes or parts of these pathways have niche-differentiating  
370 distributions (Supplementary Figure 4, Tables 2 and 3). These finer-scale differences in  
371 expression of “core” traits may explain the persistence of a diverse community when  
372 solely fed acetate, as different lineages could employ similar carbon utilization pathways  
373 differently or in more versatile ways. Another salient aspect of this analysis is the

374     astonishingly high number of possible routes within individual pathways here represented  
375     by their Disjunctive Normal Forms. For example, accounting for all alternative routes and  
376     enzymes, the glycolysis pathway has 100s of possible routes. Layering upon this many  
377     expression attributes reveals a large hidden metabolic versatility.

378     **Dimensionality of the High-Affinity Phosphorus Transporter System *PstABCS***

379         The EBPR ecosystem is characterized by its highly dynamic phosphorus cycles.  
380         To explore how different lineages respond to fluctuating phosphorus concentrations, we  
381         explored the expression-based attributes for the KEGG module of the high-affinity  
382         phosphorus transporter *pstABCS* (Figure 4). The *pstABCS* system is an ABC-type  
383         transporter that strongly binds phosphate under phosphorus-limiting conditions;  
384         therefore, it would be expected that the highest expression levels would be at the end of  
385         the aerobic cycle [72]. In contrast, we found that expression of the *pstABCS* was  
386         characterized by two different trait attributes. In the first attribute shared by 14 community  
387         members, all components of *pstABCS* displayed the highest activity towards the end of  
388         the aerobic cycle, when phosphorus concentrations were depleted (Figure 4, Attribute 1).  
389         Conversely, 11 community members displayed an alternate attribute where the highest  
390         activity of *pstABCS* was at the transition from anaerobic to aerobic phases when  
391         phosphorus concentrations are highest (Figure 4, Attribute 2).

392         These results are in agreement with previous results showing that *Accumulibacter*  
393         clade IIC has a canonical *pstABCS* expression pattern (as in Figure 4, Attribute 1) ,  
394         whereas the *Accumulibacter* clade IA has a non-canonical expression (as in Figure 4,  
395         Attribute 2) [31]. By assigning trait attributes, we are able to extend these findings beyond  
396         *Accumulibacter* to other flanking community members in the SBR ecosystem suggesting

397 that there are conserved ecological pressures driving niche differentiating expression  
398 patterns in *pstABCS* within the EBPR community.

399 **Distribution and Expression of Truncated Denitrification Steps Among EPBR  
400 Community Members**

401 Understanding the induction of denitrification is an important ecosystem property  
402 linked to the redox status of an environment. In EBPR communities, there are many  
403 diverse and incomplete denitrification pathways, distributed across many lineages  
404 denitrification steps expected in denitrifying systems (Figure 5). Among all 66 MAGs, we  
405 did not identify any single MAG with a complete denitrification pathway consisting of the  
406 genetic repertoire necessary to fully reduce nitrate to nitrogen gas (Supplementary Figure  
407 5). Instead, we identified multiple groups of organisms with truncated denitrification  
408 pathways, with steps distributed among cohorts of community members (Figure 5).

409 For the first steps of reducing nitrate to nitrite, we explored expression attributes  
410 of the *napAB* and *narGH* pathways (Figure 5B, C). For the *narGH* pathway, two attributes  
411 were identified (Figure 5B). The first *narGH* attribute was characterized by high  
412 expression in the anaerobic phase, with decreasing activity by the second time point of  
413 the anaerobic phase. Genomes containing this attribute included the experimentally  
414 verified and putative PAOs *Tetrasphaera* (TET1 and TET2) and *Ca. Obscuribacter*  
415 (OBS1), respectively. The second attribute was exhibited among members of the  
416 *Actinobacteria* (PROP2, PHYC2, PROP3, and NANO1), *Proteobacteria* (BEIJ4), and  
417 *Bacteroidetes* (BAC1). The attribute identified for *napAB* was also more highly expressed  
418 anaerobically and included CAPIA, CAPIIA, ALIC1, REYR2, RUBRI1, and BEIJ3.  
419 Interestingly, this *napAB* attribute had expression patterns that quickly decreased in the

420 first aerobic time point, suggesting a tighter regulation than Attribute 1 for *narGH*.  
421 Together, this suggests that the regulation of denitrification within the EBPR ecosystem  
422 is a niche-differentiating feature whereby the induction of denitrification pathways occurs  
423 either anaerobically or only after anaerobic carbon contact.

424 A smaller cohort contained the genetic repertoire to reduce nitrite to nitrogen gas  
425 and exhibited hallmark anaerobic-aerobic expression patterns (Figure 5E) These  
426 members within the *Proteobacteria* (OTTO2, BEIJ3, VITREO1, and ZOO1) contained the  
427 *nirS* nitrite reductase, the *norBC* nitric oxide reductase, and *nosZ*, and showed highest  
428 expression of these subunits towards the beginning of the anaerobic cycle, slowly  
429 decreasing over the aerobic period to their lowest in the end of the aerobic cycle. Although  
430 BEIJ2 was lacking the *norBC* system, it contained the *nirS* nitrite reductase and *nosZ*  
431 subunit, and exhibited similar expression patterns to others in this cohort. Other  
432 *Proteobacteria* lineages only contained the *norBC* subunits but were expressed in similar  
433 fashions (RHODO2, FLAVO1, RHIZO1, and LEAD1) (Figure 5D). Accumulibacter clades  
434 IA and IIA as well as ALIC1 were the only lineages with near-complete denitrification  
435 pathways. These lineages contained the *napAB* nitrate reductase system as mentioned  
436 above, the *nirS* nitrite reductase, *norB* (missing a confident hit for the *norC* subunit), and  
437 *nosZ*. These three lineages also exhibited hallmark upregulation of all steps in the  
438 anaerobic phase, with decreased activity after aerobic contact (Figure 5F).

439 Interestingly, Accumulibacter clade IA exhibited a higher magnitude of expression  
440 of denitrification steps when activity levels were normalized relative to clade IIA,  
441 supporting the hypothesis that denitrification is a niche-differentiating feature among  
442 clades [28, 31, 73], and possibly a strain-specific trait since denitrification traits cannot be

443 predicted based on *ppk1* clade designations [32]. For example, independent observations  
444 in differences among denitrification activities among strains within *Accumulibacter* clade  
445 IC are inconsistent [34, 74]. Within the same bioreactor environment, coexisting  
446 *Accumulibacter* clades differ between denitrification abilities and expression profiles [31,  
447 33, 75]. Truncated denitrification pathways have also been previously shown to be  
448 distributed among community members, with the complete denitrification genetic  
449 repertoire only present in few members [33, 75], which could be due to extensive  
450 horizontal gene transfer of genes comprising denitrification steps [75, 76]. Although this  
451 experiment was not conducted under denitrifying conditions, our approach could be  
452 applied to denitrifying EBPR systems to further understand the distribution of  
453 denitrification traits among community members and how to selectively enrich for diverse  
454 DPAOs.

455 **Biosynthetic Potential and Expression Dynamics of Amino Acid and Vitamin  
456 Synthesis Pathways**

457 Although SBRs are designed to enrich for *Accumulibacter* by providing acetate as  
458 the sole carbon source, a diverse flanking community persists in these setups [27, 75].  
459 One hypothesis for the persistence of flanking community members may be cooperative  
460 interactions due to underlying auxotrophies of amino acid and vitamin biosynthetic  
461 pathways in *Accumulibacter*. Amino acids and vitamin cofactors are metabolically  
462 expensive to synthesize, and widespread auxotrophies have been widely documented  
463 among microbial communities [77, 78]. Specifically, auxotrophies of vitamin cofactors  
464 have been shown to fuel bacterial and cross-kingdom interactions with *de novo* bacterial  
465 and cross-kingdom interactions with *de novo* synthesizers [79, 80]. To explore this

466 hypothesis in the EPBR SBR community, we analyzed the presence of amino acid and  
467 vitamin biosynthetic pathways and their expression patterns among the top 15 genomes  
468 based on transcript abundance (Figure 6).

469 Within *Accumulibacter*, there are a few key vitamin cofactor and amino acid  
470 auxotrophies that could fuel potential interactions with flanking community members. Both  
471 *Accumulibacter* clade genomes are missing the riboflavin pathway for FAD cofactor  
472 synthesis, as well as the pathways for serine and aspartic acid (Figure 6A). The  
473 biosynthetic pathway for aspartic acid is distributed among members of the *Bacteroidetes*  
474 and *Proteobacteria*, whereas only TET2 contains the pathway for serine synthesis (Figure  
475 5A). The lack of serine biosynthesis pathways in *Accumulibacter* and other flanking  
476 genomes seems striking given that serine is one of the least metabolically costly amino  
477 acids to synthesize [81]. Interestingly, *Accumulibacter* clade IIA does not contain the  
478 biosynthetic machinery for thiamine and pantothenate synthesis, whereas clade IA does  
479 (Figure 6A). Only the CAULO1, HYPHO1, and PSEUDO1 genomes within the  
480 *Proteobacteria* can synthesize thiamine, whereas several other members can synthesize  
481 pantothenate (Figure 6A). The absence of the pantothenate biosynthetic pathway in  
482 *Accumulibacter* CAP IIA is particularly interesting given that coenzyme A is essential for  
483 polyhydroxyalkanoate biosynthesis, which fuels the polymer cycling PAO phenotype of  
484 *Accumulibacter* [24].

485 In addition to flanking community members potentially supporting the growth of  
486 *Accumulibacter* due to underlying auxotrophies, the reciprocal logic may be possible as  
487 well. Both *Accumulibacter* clades contain the pathways for synthesizing tyrosine and  
488 phenylalanine, which are missing in a majority of the top 15 active flanking genomes

489 (Figure 6A). Only two other members within the *Proteobacteria* can synthesize tyrosine  
490 and phenylalanine, where RAM1 can synthesize both and PSEUDO1 only phenylalanine.  
491 Interestingly, phenylalanine and tyrosine are the second and third most metabolically  
492 expensive amino acids to synthesize, respectively, with tryptophan the most costly [81].  
493 Additionally, a few highly active flanking community members lack the biosynthetic  
494 machinery for several vitamin cofactors and amino acids, such as FLAVO1 and BAC3  
495 within the *Bacteroidetes* and the putative PAO *Ca. Obscuribacter phosphatis* OBS1  
496 (Figure 6A). Particularly, RAM1 within the *Proteobacteria* is missing the biosynthetic  
497 machinery for all vitamin cofactors but can synthesize most amino acids including the  
498 most metabolically expensive as mentioned above.

499 We next analyzed the distribution of trait-attributes of vitamin and amino acid  
500 pathways among these genomes to understand how these biosynthetic pathways are  
501 expressed similarly or differently in the EBPR SBR ecosystem (Figure 6B and C).  
502 Members of the *Proteobacteria* containing thiamine and cobalamin biosynthetic pathways  
503 all express these traits similarly (Figure 6B). However, the pantothenate synthesis  
504 pathway contains two trait-attributes and is expressed differently among two cohorts. In  
505 the first attribute, RUN1, TET1, CAULO1, CAPIA, and PSEUDO1 express the  
506 pantothenate pathway similarly. However, OBS1 and TET2 express the pantothenate  
507 pathway differently (Figure 6B). Because tetrahydrofolate can be synthesized through  
508 different metabolic routes, we analyzed the differences in trait attribute expression for all  
509 routes in genomes that contained sufficient coverage of this trait. Members of the  
510 *Bacteroidetes* and *Proteobacteria* mostly cluster together among tetrahydrofolate  
511 attributes, whereas the TET1 and TET2 genomes are differentiated (Figure 6B).

512 Expression of various groups of amino acids show more differentiated patterns of  
513 expression for genomes with these pathways. Several amino acids also contain different  
514 metabolic routes for biosynthesis, and we analyzed all trait attributes for each amino acid  
515 for all routes grouped by type (Figure 6C). For the charged amino acids arginine, histidine,  
516 and lysine, members of the *Proteobacteria* and *Bacteroidetes* cluster within their  
517 phylogenetic groups, respectively, with lysine and histidine expressed differently among  
518 these groups (Figure 6C). In contrast, arginine is expressed similarly among all  
519 *Proteobacteria* genomes. Among the polar charged amino acids, TET2 is the only  
520 genome among the top 15 genomes that contains the metabolic pathway to synthesize  
521 serine (Figure 6A). Several groups contain the pathway for threonine synthesis, and  
522 expression of different threonine routes are differentiated among the *Proteobacteria*,  
523 *Bacteroidetes*, and *Tetrasphaera spp.*, but mostly clusters phylogenetically (Figure 6C).  
524 Notably, the expression patterns for the cysteine and proline biosynthetic pathways do  
525 not cluster phylogenetically, such as both *Tetrasphaera* genomes expressing the proline  
526 pathway more similarly to other *Proteobacteria* and *Bacteroidetes* (Figure 6C). The few  
527 lineages that can synthesize tyrosine and phenylalanine (CAPIA, CAPIIA, RAM1,  
528 PSEUDO1) show different patterns of expression. These results show that beyond the  
529 presence or absence of key vitamin cofactor and amino acid biosynthetic pathways,  
530 EBPR SBR organisms also display coherent and differentiated patterns of expression for  
531 these traits, of which the functional consequences remain to be further understood.

532

533

534

## 535 CONCLUSIONS AND FUTURE PERSPECTIVES

536 In this work, we applied a novel trait-based 'omics pipeline to a semi-complex,  
537 engineered bioreactor microbial community to explore ecosystem-level and niche-  
538 differentiating traits. Through assembling high-quality MAGs of the EBPR SBR  
539 community and using a time-series metatranscriptomics experiment, we were able to  
540 extend functional predictions and ecosystem inferences beyond hypotheses made from  
541 gene presence/absence data. Using our novel trait-based comparative 'omics pipeline,  
542 we identified how similarities and differences in the expression of significant EBPR traits  
543 are conferred among community members such as phosphorus cycling, denitrification,  
544 and amino acid metabolism. Specifically, we demonstrate that traits with similar  
545 expression profiles may be clustered into attributes providing a new layer to trait-based  
546 approaches.

547 We believe that identifying expression-based attributes will be a powerful tool to  
548 explore microbial traits in natural, engineered, and host-associated microbiomes. Outside  
549 of activated sludge systems, trait-based approaches could illuminate how similar  
550 secondary metabolite clusters are expressed among different species in a community [82,  
551 83], how auxotrophies for amino acid and vitamin cofactors govern interactions [84], how  
552 rhizosphere microorganisms respond to day-night cycles, and identify putative traits that  
553 universally exhibit ecosystem-level or niche-differentiating patterns across ecosystems  
554 [19, 23]. Importantly, our trait-based approach can be used to screen for expected  
555 expression patterns of a key trait compared to a model organism, and then prioritize  
556 specific microbial lineages for downstream experimental verification with techniques such  
557 as Raman-FISH [85, 86]. Overall, our trait-based comparative 'omics pipeline is a novel

558 and high-throughput approach to understand how microbial traits connect to ecosystem-  
559 level processes in diverse microbiomes.

560

## 561 **ACKNOWLEDGEMENTS**

562 We thank Caitlin Singleton for providing early access to high-quality genomes from  
563 a full-scale WWTP to compare our MAGs against. Metagenomic and metatranscriptomic  
564 sequencing was provided through a Joint Genome Institute Community Science Proposal  
565 (Proposal ID 873). This work was supported by funding from the National Science  
566 Foundation (MCB-1518130) to K.D.M and D.R.N. Funding was provided to E.A.M. by a  
567 fellowship through the Department of Bacteriology at the University of Wisconsin –  
568 Madison. Funding for B.O.O was in part provided by the Technology Foundation of the  
569 Dutch National Science Foundation (NWO-TTW). This research was performed in part  
570 using the Wisconsin Energy Institute computing cluster, which is supported by the Great  
571 Lakes Bioenergy Research Center as a part of the U.S. Department of Energy Office of  
572 Science (DE-SC0018409).

573

574

575

576

577

578

579

580

581 **REFERENCES CITED**

582 1. Violette C, Navas M-L, Vile D, Kazakou E, Fortunel C, Hummel I, et al. Let the  
583 concept of trait be functional! *Oikos* 2007; **116**: 882–892.

584 2. Lavorel S, Garnier E. Predicting changes in community composition and  
585 ecosystem functioning from plant traits: revisiting the Holy Grail. *Funct Ecol* 2002;  
586 **16**: 545–556.

587 3. Hooper DU, Chapin FS, Ewel JJ, Hector A, Inchausti P, Lavorel S, et al.  
588 EFFECTS OF BIODIVERSITY ON ECOSYSTEM FUNCTIONING: A  
589 CONSENSUS OF CURRENT KNOWLEDGE. *Ecol Monogr* 2005; **75**: 3–35.

590 4. Pianka ER. On r-and K-Selection. *Am Nat* 1970.

591 5. Wright IJ, Reich PB, Westoby M, Ackerly DD, Baruch Z, Bongers F, et al. The  
592 worldwide leaf economics spectrum. *Nature* 2004; **428**: 821–827.

593 6. Krause S, Le Roux X, Niklaus PA, Van Bodegom PM, Lennon JT, Bertilsson S, et  
594 al. Trait-based approaches for understanding microbial biodiversity and  
595 ecosystem functioning. *Front Microbiol* 2014; **5**: 251.

596 7. Malik AA, Martiny JBH, Brodie EL, Martiny AC, Treseder KK, Allison SD, et al.  
597 Defining trait-based microbial strategies with consequences for soil carbon cycling  
598 under climate change. *bioRxiv* 2019.

599 8. Gittar J, Shade A, Litchman E. Trait-based community assembly and succession  
600 of the infant gut microbiome. *Nat Commun* 2019; **10**: 512.

601 9. Wolfe BE, Button JE, Santarelli M, Dutton RJ. Cheese Rind Communities Provide  
602 Tractable Systems for In Situ and In Vitro Studies of Microbial Diversity. *Cell*  
603 2014; **158**: 422–433.

604 10. Enke TN, Datta MS, Schwartzman J, Barrere J, Pascual-García A, Cordero  
605 Correspondence OX. Modular Assembly of Polysaccharide-Degrading Marine  
606 Microbial Communities. *Curr Biol* 2019; **29**.

607 11. Herrera Paredes S, Gao T, Law TF, Finkel OM, Mucyn T, Teixeira PJPL, et al.  
608 Design of synthetic bacterial communities for predictable plant phenotypes. *PLOS  
609 Biol* 2018; **16**: e2003962.

610 12. Lindemann SR, Bernstein HC, Song H-S, Fredrickson JK, Fields MW, Shou W, et  
611 al. Engineering microbial consortia for controllable outputs. *ISME J* 2016; **10**:  
612 2077–2084.

613 13. Oyserman BO, Medema MH, Raaijmakers JM. Road MAPs to engineer host  
614 microbiomes. *Curr Opin Microbiol* 2018; **43**: 46–54.

615 14. Lawson CE, Harcombe WR, Hatzenpichler R, Lindemann SR, Löffler FE,  
616 O’Malley MA, et al. Common principles and best practices for engineering  
617 microbiomes. *Nat Rev Microbiol* . 2019. Nature Publishing Group. , **17**: 725–741

618 15. Gutierrez CF, Sanabria J, Raaijmakers JM, Oyserman BO. Restoring degraded  
619 microbiome function with self-assembled communities. *FEMS Microbiol Ecol*  
620 2020; **96**.

621 16. Allison SD. A trait-based approach for modelling microbial litter decomposition.  
622 *Ecol Lett* 2012; **15**: 1058–1070.

623 17. Tringe SG, von Mering C, Kobayashi A, Salamov AA, Chen K, Chang HW, et al.  
624 Comparative metagenomics of microbial communities. *Science* 2005; **308**: 554–7.

625 18. Tyson GW, Chapman J, Hugenholtz P, Allen EE, Ram RJ, Richardson PM, et al.  
626 Community structure and metabolism through reconstruction of microbial

627 genomes from the environment. *Nature* 2004; **428**: 37–43.

628 19. Anantharaman K, Brown CT, Hug LA, Sharon I, Castelle CJ, Probst AJ, et al.

629 Thousands of microbial genomes shed light on interconnected biogeochemical

630 processes in an aquifer system. *Nat Commun* 2016; **7**: 13219.

631 20. Woodcroft BJ, Singleton CM, Boyd JA, Evans PN, Emerson JB, Zayed AAF, et al.

632 Genome-centric view of carbon processing in thawing permafrost. *Nature* 2018;

633 **560**: 49–54.

634 21. Albertsen M, Hugenholtz P, Skarszewski A, Nielsen KL, Tyson GW, Nielsen PH.

635 Genome sequences of rare, uncultured bacteria obtained by differential coverage

636 binning of multiple metagenomes. *Nat Biotechnol* 2013; **31**: 533–538.

637 22. Anantharaman K, Brown CT, Hug LA, Sharon I, Castelle CJ, Probst AJ, et al.

638 Thousands of microbial genomes shed light on interconnected biogeochemical

639 processes in an aquifer system. *Nat Commun* 2016; **7**: 13219.

640 23. Wrighton KC, Thomas BC, Sharon I, Miller CS, Castelle CJ, VerBerkmoes NC, et

641 al. Fermentation, hydrogen, and sulfur metabolism in multiple uncultivated

642 bacterial phyla. *Science* 2012; **337**: 1661–5.

643 24. Hesselmann RPX, Werlen C, Hahn D, van der Meer JR, Zehnder AJB.

644 Enrichment, Phylogenetic Analysis and Detection of a Bacterium That Performs

645 Enhanced Biological Phosphate Removal in Activated Sludge. *Syst Appl Microbiol*

646 1999; **22**: 454–465.

647 25. Seviour RJ, Mino T, Onuki M. The microbiology of biological phosphorus removal

648 in activated sludge systems. *FEMS Microbiol Rev* 2003; **27**: 99–127.

649 26. Crocetti GR, Hugenholtz P, Bond PL, Schuler A, Ju J, Keller J, et al. Identification

650 of Polyphosphate-Accumulating Organisms and Design of 16S rRNA-Directed  
651 Probes for Their Detection and Quantitation. *APPLIED AND ENVIRONMENTAL*  
652 *MICROBIOLOGY*. 2000.

653 27. Martín HG, Ivanova N, Kunin V, Warnecke F, Barry KW, McHardy AC, et al.  
654 Metagenomic analysis of two enhanced biological phosphorus removal (EBPR)  
655 sludge communities. *Nat Biotechnol* 2006; **24**: 1263–1269.

656 28. Flowers JJ, He S, Malfatti S, del Rio TG, Tringe SG, Hugenholtz P, et al.  
657 Comparative genomics of two 'Candidatus Accumulibacter' clades performing  
658 biological phosphorus removal. *ISME J* 2013; **7**: 2301–2314.

659 29. Oyserman BO, Moya F, Lawson CE, Garcia AL, Vogt M, Heffernan M, et al.  
660 Ancestral genome reconstruction identifies the evolutionary basis for trait  
661 acquisition in polyphosphate accumulating bacteria. *ISME J* 2016; **10**: 2931–  
662 2945.

663 30. Wilmes P, Andersson AF, Lefsrud MG, Wexler M, Shah M, Zhang B, et al.  
664 Community proteogenomics highlights microbial strain-variant protein expression  
665 within activated sludge performing enhanced biological phosphorus removal.  
666 *ISME J* 2008; **2**: 853–864.

667 31. McDaniel E, Moya-Flores F, Keene Beach N, Oyserman B, Kizaric M, Hoe Khor  
668 E, et al. Metabolic differentiation of co-occurring Accumulibacter clades revealed  
669 through genome-resolved metatranscriptomics. *bioRxiv* 2020;  
670 2020.11.23.394700.

671 32. Gao H, Mao Y, Zhao X, Liu WT, Zhang T, Wells G. Genome-centric  
672 metagenomics resolves microbial diversity and prevalent truncated denitrification

673 pathways in a denitrifying PAO-enriched bioprocess. *Water Res* 2019; **155**: 275–  
674 287.

675 33. Wang Y, Gao H, Wells G. Integrated Omics Analyses Reveal Differential Gene  
676 Expression and Potential for Cooperation Between Denitrifying Polyphosphate  
677 and Glycogen Accumulating Organisms. *bioRxiv* . 2020. bioRxiv. ,  
678 2020.01.10.901413

679 34. Camejo PY, Oyserman BO, McMahon KD, Noguera DR. Integrated Omic  
680 Analyses Provide Evidence that a 'Candidatus Accumulibacter phosphatis' Strain  
681 Performs Denitrification under Microaerobic Conditions. *mSystems* 2019; **4**:  
682 e00193-18.

683 35. Kong Y, Nielsen JL, Nielsen PH. Identity and ecophysiology of uncultured  
684 actinobacterial polyphosphate-accumulating organisms in full-scale enhanced  
685 biological phosphorus removal plants. *Appl Environ Microbiol* 2005; **71**: 4076–85.

686 36. Kristiansen R, Nguyen HTT, Saunders AM, Nielsen JL, Wimmer R, Le VQ, et al.  
687 A metabolic model for members of the genus *Tetrasphaera* involved in enhanced  
688 biological phosphorus removal. *ISME J* 2013; **7**: 543–54.

689 37. Soo R, Skennerton CT, Sekiguchi Y, Imelfort M, Paech S, Dennis P, et al. An  
690 Expanded Genomic Representation of the Phylum Cyanobacteria. *Genome*  
691 *Biology and Evolution*. <https://www.ncbi.nlm.nih.gov/pmc/articles/PMC4040986/>.  
692 Accessed 11 Jul 2020.

693 38. Petriglieri F, Singleton C, Pece M, Petersen JF, Nierychlo M, Nielsen H.  
694 'Candidatus Dechloromonas phosphatis' and 'Candidatus Dechloromonas  
695 phosphovora', two novel polyphosphate accumulating organisms abundant in

696 wastewater treatment systems. *bioRxiv* 2020.

697 39. Singleton CM, Petriglieri F, Kristensen JM, Kirkegaard RH, Michaelsen TY,  
698 Andersen MH, et al. Connecting structure to function with the recovery of over  
699 1000 high-quality metagenome-assembled genomes from activated sludge using  
700 long-read sequencing. *Nat Commun* 2021; **12**: 2009.

701 40. Oyserman BO, Noguera DR, del Rio TG, Tringe SG, McMahon KD.  
702 Metatranscriptomic insights on gene expression and regulatory controls in  
703 *Candidatus Accumulibacter phosphatis*. *ISME J* 2016; **10**: 810–822.

704 41. Parks DH, Imelfort M, Skennerton CT, Hugenholtz P, Tyson GW. CheckM:  
705 assessing the quality of microbial genomes recovered from isolates, single cells,  
706 and metagenomes. *Genome Res* 2015; **25**: 1043–55.

707 42. Kanehisa M, Sato Y, Morishima K. BlastKOALA and GhostKOALA: KEGG Tools  
708 for Functional Characterization of Genome and Metagenome Sequences. *J Mol  
709 Biol* 2016; **428**: 726–731.

710 43. Aramaki T, Blanc-Mathieu R, Endo H, Ohkubo K, Kanehisa M, Goto S, et al.  
711 KofamKOALA: KEGG ortholog assignment based on profile HMM and adaptive  
712 score threshold. *bioRxiv* 2019; 602110.

713 44. Bushnell B, Rood J, Singer E. BBMerge – Accurate paired shotgun read merging  
714 via overlap. *PLoS One* 2017; **12**: e0185056.

715 45. Kopylova E, Noé L, Touzet H. SortMeRNA: fast and accurate filtering of ribosomal  
716 RNAs in metatranscriptomic data. *Bioinformatics* 2012; **28**: 3211–3217.

717 46. Bray NL, Pimentel H, Melsted P, Pachter L. Near-optimal probabilistic RNA-seq  
718 quantification. *Nat Biotechnol* 2016; **34**: 525–527.

719 47. Soneson C, Love MI, Robinson MD. Differential analyses for RNA-seq: transcript-  
720 level estimates improve gene-level inferences. *F1000Research* 2015; **4**: 1521.

721 48. Jain C, Rodriguez-R LM, Phillippy AM, Konstantinidis KT, Aluru S. High  
722 throughput ANI analysis of 90K prokaryotic genomes reveals clear species  
723 boundaries. *Nat Commun* 2018; **9**: 5114.

724 49. He S, Gall DL, McMahon KD. 'Candidatus accumulibacter' population structure in  
725 enhanced biological phosphorus removal sludges as revealed by polyphosphate  
726 kinase genes. *Appl Environ Microbiol* 2007; **73**: 5865–5874.

727 50. Camejo PY, Owen BR, Martirano J, Ma J, Kapoor V, Santo Domingo J, et al.  
728 *Candidatus Accumulibacter phosphatis* clades enriched under cyclic anaerobic  
729 and microaerobic conditions simultaneously use different electron acceptors.  
730 *Water Res* 2016; **102**: 125–137.

731 51. Zhang H, Sekiguchi Y, Hanada S, Hugenholtz P, Kim H, Kamagata Y, et al.  
732 *Gemmatumonas aurantiaca* gen. nov., sp. nov., a Gram-negative, aerobic,  
733 polyphosphate-accumulating micro-organism, the first cultured representative of  
734 the new bacterial phylum *Gemmatumonadetes* phyl. nov. *Int J Syst Evol Microbiol*  
735 2003; **53**: 1155–1163.

736 52. McDaniel EA, Wever R, Oyserman BO, Noguera DR, McMahon KD. Genome-  
737 Resolved Metagenomics of a Photosynthetic Bioreactor Performing Biological  
738 Nutrient Removal. *Microbiol Resour Announc* 2021; **10**.

739 53. Speirs LBM, Rice DTF, Petrovski S, Seviour RJ. The Phylogeny, Biodiversity, and  
740 Ecology of the Chloroflexi in Activated Sludge. *Front Microbiol* . 2019. Frontiers  
741 Media S.A. , **10**: 2015

742 54. Andersen MH, McIlroy SJ, Nierychlo M, Nielsen PH, Albertsen M. Genomic  
743 insights into *Candidatus Amarolinea aalborgensis* gen. nov., sp. nov., associated  
744 with settleability problems in wastewater treatment plants. *Syst Appl Microbiol*  
745 2019; **42**: 77–84.

746 55. Nierychlo M, Miłobędzka A, Petriglieri F, McIlroy B, Nielsen PH, McIlroy SJ. The  
747 morphology and metabolic potential of the Chloroflexi in full-scale activated  
748 sludge wastewater treatment plants. *FEMS Microbiol Ecol* 2019; **95**.

749 56. McIlroy SJ, Karst SM, Nierychlo M, Dueholm MS, Albertsen M, Kirkegaard RH, et  
750 al. Genomic and in situ investigations of the novel uncultured Chloroflexi  
751 associated with 0092 morphotype filamentous bulking in activated sludge. *ISME J*  
752 2016; **10**: 2223–2234.

753 57. Kragelund C, Levantesi C, Borger A, Thelen K, Eikelboom D, Tandoi V, et al.  
754 Identity, abundance and ecophysiology of filamentous Chloroflexi species present  
755 in activated sludge treatment plants. *FEMS Microbiol Ecol* 2007; **59**: 671–682.

756 58. Kindaichi T, Yamaoka S, Uehara R, Ozaki N, Ohashi A, Albertsen M, et al.  
757 Phylogenetic diversity and ecophysiology of Candidate phylum Saccharibacteria  
758 in activated sludge. *FEMS Microbiol Ecol* 2016; **92**: 1–11.

759 59. Mann E, Wetzels SU, Wagner M, Zebeli Q, Schmitz-Esser S. Metatranscriptome  
760 Sequencing Reveals Insights into the Gene Expression and Functional Potential  
761 of Rumen Wall Bacteria. *Front Microbiol* 2018; **9**: 43.

762 60. Jiang Y, Xiong X, Danska J, Parkinson J. Metatranscriptomic analysis of diverse  
763 microbial communities reveals core metabolic pathways and microbiome-specific  
764 functionality. *Microbiome* 2016; **4**: 2.

765 61. Linz AM, Aylward FO, Bertilsson S, McMahon KD. Time-series  
766 metatranscriptomes reveal conserved patterns between phototrophic and  
767 heterotrophic microbes in diverse freshwater systems. *Limnol Oceanogr* 2019.

768 62. Lawson CE, Wu S, Bhattacharjee AS, Hamilton JJ, McMahon KD, Goel R, et al.  
769 Metabolic network analysis reveals microbial community interactions in anammox  
770 granules. *Nat Commun* 2017; **8**: 15416.

771 63. Aylward FO, Eppley JM, Smith JM, Chavez FP, Scholin CA, DeLong EF.  
772 Microbial community transcriptional networks are conserved in three domains at  
773 ocean basin scales. *Proc Natl Acad Sci* 2015; **112**: 5443–5448.

774 64. Hao L, Michaelsen TY, Singleton CM, Dottorini G, Kirkegaard RH, Albertsen M, et  
775 al. Novel syntrophic bacteria in full-scale anaerobic digesters revealed by  
776 genome-centric metatranscriptomics. *ISME J* 2020; **14**: 906–918.

777 65. Glass EM, Meyer F. The Metagenomics RAST Server: A Public Resource for the  
778 Automatic Phylogenetic and Functional Analysis of Metagenomes. *Handb Mol  
779 Microb Ecol I Metagenomics Complement Approaches* 2011; **8**: 325–331.

780 66. Martinez X, Pozuelo M, Pascal V, Campos D, Gut I, Gut M, et al. MetaTrans: an  
781 open-source pipeline for metatranscriptomics. *Sci Rep* 2016; **6**: 26447.

782 67. Westreich ST, Treiber ML, Mills DA, Korf I, Lemay DG. SAMSA2: a standalone  
783 metatranscriptome analysis pipeline. *BMC Bioinformatics* 2018; **19**: 175.

784 68. Ni Y, Li J, Panagiotou G. COMAN: a web server for comprehensive  
785 metatranscriptomics analysis. *BMC Genomics* 2016; **17**: 622.

786 69. Narayanasamy S, Jarosz Y, Muller EEL, Heintz-Buschart A, Herold M, Kaysen A,  
787 et al. IMP: a pipeline for reproducible reference-independent integrated

788 metagenomic and metatranscriptomic analyses. *Genome Biol* 2016; **17**: 260.

789 70. Eren AM, Esen ÖC, Quince C, Vineis JH, Morrison HG, Sogin ML, et al. Anvi'o:  
790 an advanced analysis and visualization platform for 'omics data. *PeerJ* 2015; **3**:  
791 e1319.

792 71. Kanehisa M, Sato Y, Kawashima M, Furumichi M, Tanabe M. KEGG as a  
793 reference resource for gene and protein annotation. *Nucleic Acids Res* 2016; **44**:  
794 D457–D462.

795 72. Wanner BL. Gene regulation by phosphate in enteric bacteria. *J Cell Biochem*  
796 1993; **51**: 47–54.

797 73. Flowers JJ, He S, Yilmaz S, Noguera DR, McMahon KD. Denitrification  
798 capabilities of two biological phosphorus removal sludges dominated by different  
799 'Candidatus Accumulibacter' clades. *Environ Microbiol Rep* 2009; **1**: 583–588.

800 74. Rubio-Rincón FJ, Weissbrodt DG, Lopez-Vazquez CM, Welles L, Abbas B,  
801 Albertsen M, et al. 'Candidatus Accumulibacter delftensis': A clade IC novel  
802 polyphosphate-accumulating organism without denitrifying activity on nitrate.  
803 *Water Res* 2019; **161**: 136–151.

804 75. Gao H, Mao Y, Zhao X, Liu WT, Zhang T, Wells G. Genome-centric  
805 metagenomics resolves microbial diversity and prevalent truncated denitrification  
806 pathways in a denitrifying PAO-enriched bioprocess. *Water Res* 2019; **155**: 275–  
807 287.

808 76. Parsons C, Stüeken EE, Rosen CJ, Mateos K, Anderson RE. Radiation of  
809 nitrogen-metabolizing enzymes across the tree of life tracks environmental  
810 transitions in Earth history. *Geobiology* 2020.

811 77. Gómez-Consarnau L, Sachdeva R, Gifford SM, Cutter LS, Fuhrman JA, Sañudo-  
812 Wilhelmy SA, et al. Mosaic patterns of B-vitamin synthesis and utilization in a  
813 natural marine microbial community. *Environ Microbiol* 2018; **20**: 2809–2823.

814 78. Hamilton JJ, Garcia SL, Brown BS, Oyserman BO, Moya-Flores F, Bertilsson S,  
815 et al. Metabolic Network Analysis and Metatranscriptomics Reveal Auxotrophies  
816 and Nutrient Sources of the Cosmopolitan Freshwater Microbial Lineage *acl*.  
817 *mSystems* 2017; **2**: e00091-17.

818 79. McClure RS, Overall CC, Hill EA, Song H-S, Charania M, Bernstein HC, et al.  
819 Species-specific transcriptomic network inference of interspecies interactions.  
820 *ISME J* 2018; **1**.

821 80. Croft MT, Lawrence AD, Raux-Deery E, Warren MJ, Smith AG. Algae acquire  
822 vitamin B12 through a symbiotic relationship with bacteria. *Nature* 2005; **438**: 90–  
823 93.

824 81. Akashi H, Gojobori T. Metabolic efficiency and amino acid composition in the  
825 proteomes of *Escherichia coli* and *Bacillus subtilis*. *Proc Natl Acad Sci U S A*  
826 2002; **99**: 3695–3700.

827 82. Lozano GL, Bravo JI, Diago MFG, Park HB, Hurley A, Peterson SB, et al.  
828 Introducing THOR, a Model Microbiome for Genetic Dissection of Community  
829 Behavior. *MBio* 2019; **10**: e02846-18.

830 83. Crits-Christoph A, Diamond S, Butterfield CN, Thomas BC, Banfield JF. Novel soil  
831 bacteria possess diverse genes for secondary metabolite biosynthesis. *Nature*  
832 2018; **558**: 440–444.

833 84. Zengler K, Zaramela LS. The social network of microorganisms — how

834 auxotrophies shape complex communities. *Nat Rev Microbiol* 2018; **16**: 383–390.

835 85. Fernando EY, McIlroy SJ, Nierychlo M, Herbst FA, Petriglieri F, Schmid MC, et al.

836 Resolving the individual contribution of key microbial populations to enhanced

837 biological phosphorus removal with Raman–FISH. *ISME J* 2019; **13**: 1933–1946.

838 86. Petriglieri F, Petersen JF, Peces M, Nierychlo M, Hansen K, Baastrand CE, et al.

839 Quantification of biologically and chemically bound phosphorus in activated

840 sludge from full-scale plants with biological P-removal. *bioRxiv* 2021.

841 87. Chaumeil P-A, Mussig AJ, Hugenholtz P, Parks DH. GTDB-Tk: a toolkit to classify

842 genomes with the Genome Taxonomy Database. *Bioinformatics* 2019.

843 88. Seemann T. Prokka: Rapid prokaryotic genome annotation. *Bioinformatics* 2014;

844 **30.**

845

846

847

848

849

850

851

852

853

854

855

856

857 **FIGURE AND TABLE LEGENDS**

858 **Figure 1. Overview of Trait-based Comparative Transcriptomics Approach**

859 In genome-resolved metagenomics approaches, representative MAGs are assembled  
860 from a microbial community of interest, and the presence and/or absence of key metabolic  
861 pathways are used to make inferences of metabolic potential and ecosystem processes.  
862 However, metagenomic data alone can only assess the metabolic potential of a given  
863 pathway, and do not provide other biologically relevant information such as the timing or  
864 induction of these traits. Using time-series metatranscriptomics, we developed a trait-  
865 based comparative ‘omics (TbasCO) pipeline that statistically assesses the inter-  
866 organismal differences in gene expression pattern of a given trait to cluster into trait  
867 attributes.

868

869 **Figure 2. Genome-Resolved Metatranscriptomics Approach of an EBPR System**

870 Application of a genome-resolved metatranscriptomics approach to a lab-scale  
871 sequencing batch reactor (SBR) designed to enrich for *Accumulibacter*. **1A)** Schematic  
872 of the main cycle parameters and analyte dynamics of an SBR simulating EBPR. Six  
873 samples were taken for RNA sequencing within the cycle at time-points denoted by  
874 arrows. **1B)** Phylogenetic identity and abundance patterns of 66 assembled MAGs from  
875 the EBPR system. The phylogenetic tree was constructed from concatenated markers  
876 contained in the GTDB-tk with muscle, calculated with RAxML, and visualized in iTOL. A  
877 phylogenetic tree of all 66 MAGs with reference genomes and high-quality genomes from  
878 Singleton et al. constructed with concatenated markers from GTDB-tk are provided in  
879 Supplementary Figure 1. Sizes of circles represent abundance patterns of metagenomic

880 reads mapping back to genomes from the same day as the metatranscriptomic  
881 experiment and are not to scale. **1C)** Transcriptional patterns of each MAG in the  
882 anaerobic and aerobic phases of the EBPR cycle. RNA-seq reads from each time-point  
883 were competitively mapped to all 66 assembled MAGs and counts normalized by  
884 transcripts per million (TPM). Total counts in the anaerobic and aerobic phases for each  
885 genome were averaged separately and plotted on a log scale. Order of MAGs from left to  
886 right mirrors the order of MAGs in the phylogenetic tree in 1B from the top of the circle  
887 going clockwise.

888

889 **Figure 3. Clustering and Distribution of Trait Attributes Across EBPR SBR**  
890 **Community Members.** Using the TbasCO method, we identified expression-based trait  
891 attributes from predefined trait modules in the KEGG library and explored the distribution  
892 of these trait attributes across community members. **A)** Distribution of trait-attributes  
893 among sets of genomes. Bars represent the number of trait-attributes present in a set  
894 number of genomes and colored by KEGG module category. Among a total of 35  
895 genomes, trait attributes present between 3-18 genomes are designated as niche  
896 differentiating, whereas trait attributes present in 19 or greater genomes are designated  
897 as core trait attributes. Inset figure demonstrates the maximum number of attributes for  
898 the maximum number of genomes. **B)** Cytoscape network showing the connectedness of  
899 genomes to trait attributes. The network was filtered to only include nodes with more than  
900 5 connections, therefore filtering out both genomes with few trait attributes and trait  
901 attributes connected to less than 5 genomes. Genomes are represented as squares  
902 colored by phylum, and trait attributes are represented as circles colored by KEGG

903 category. The size of both the squares and circles represents the number of connections  
904 to that genome or trait attribute, respectively.

905

906 **Figure 4. Trait Attributes of the High-Affinity Phosphorus Transporter System**

907 ***pstABCS***

908 Using the TbasCO method, two trait attributes of the high-affinity phosphorus transporter  
909 system *pstABCS* were identified. The *pstABCS* system consists of a phosphate-binding  
910 protein and ABC-type transporter, and the corresponding KEGG orthologs for each  
911 subunit are shown. Timepoints 1-3 refer to the three anaerobic phase timepoints, and  
912 timepoints 4-6 refer to the three aerobic phase timepoints (Figure 1). Expression values  
913 are log-transformed based on setting the lowest expression value within each genome  
914 across the time-series to 0 for each subunit. Specific subunits for some genomes in both  
915 attributes are missing to the high cutoff thresholds for annotations. However we kept  
916 genomes with 2/4 subunits to show similarities in expression profiles. The first *pstABCS*  
917 trait-attribute includes microbial lineages that exhibited the highest expression of all  
918 subunits towards the end of the aerobic cycle, when phosphate concentrations are  
919 expected to be lowest. This includes microbial lineages within the *Actinobacteria*,  
920 *Proteobacteria*, *Gemmatimonadetes*, and *Chloroflexi*. The second *pstABCS* trait-attribute  
921 includes lineages that exhibited highest expression of all subunits upon the switch from  
922 anaerobic to aerobic phases, or when phosphate concentrations are expected to be the  
923 highest. This includes lineages within the *Actinobacteria* and *Proteobacteria*.

924

925 **Figure 5. Expression Dynamics of Distributed Denitrification Routes**

926 Expression of denitrification traits distributed among community members in the EBPR  
927 SBR ecosystem. Timepoints 1-3 correspond to the anaerobic phase and timepoints 4-6  
928 correspond to the aerobic phase as referenced in Figure 1. **A)** Complete denitrification  
929 pathway and associated genetic repertoire with each sequential step. **B)** Trait attributes  
930 of expression dynamics for community members with the *narGH* nitrate reductase  
931 system. This trait was the only denitrification trait identified with more than one attribute.  
932 **C)** Expression dynamics of the *napAB* nitrate reductase system. **D)** Expression dynamics  
933 of the *norBC* nitrous oxide reductase system. **E)** Expression of all steps of denitrification  
934 starting at nitrite reduction. **F)** Expression of the most complete denitrification route  
935 among three community members, with the *norC* subunit for nitrous oxide reduction  
936 missing. Note that OTTO1 only contains *nirS* but is included in this trait attribute because  
937 the expression dynamics are similar to that of the other three genomes for this subunit.

938

939 **Figure 6. Biosynthetic Potential Compared to Expression of Amino Acid and**  
940 **Vitamin Synthesis Pathways for Top 15 Expressed MAGs**

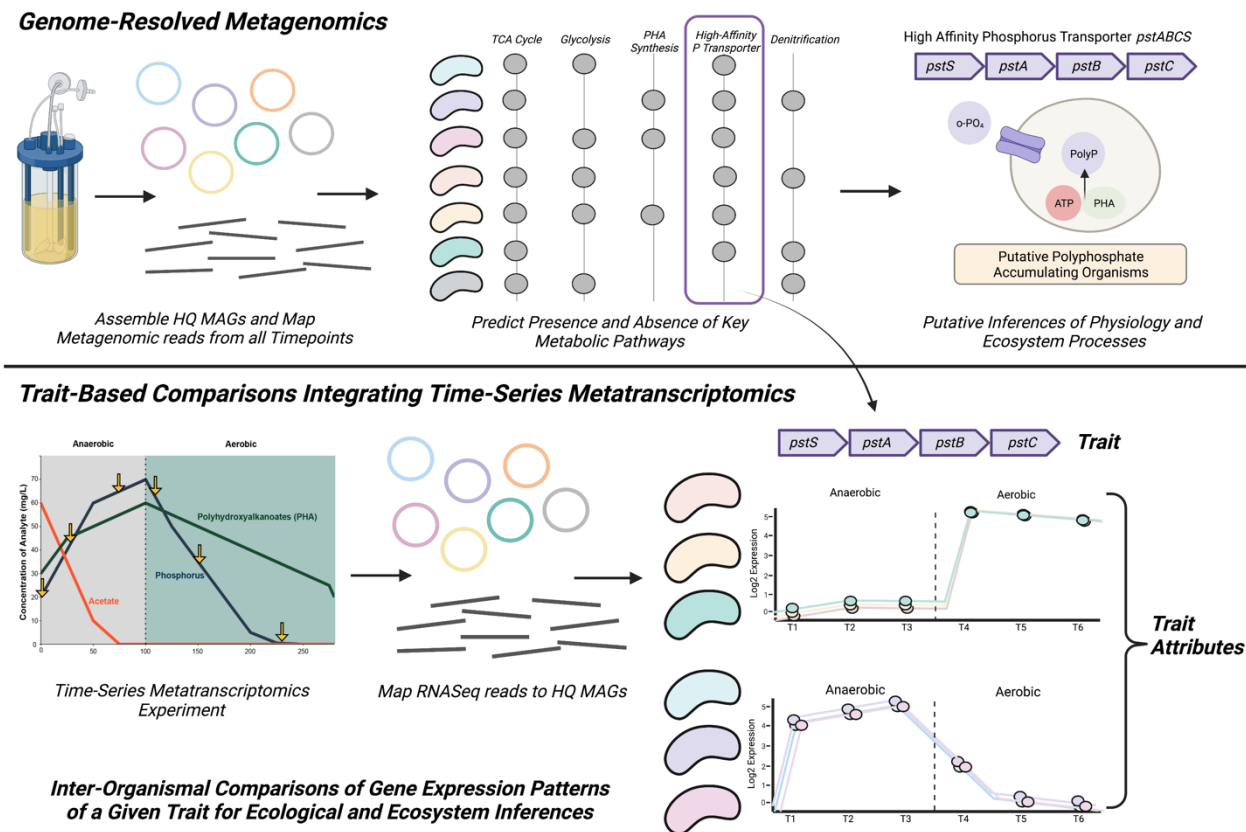
941 Biosynthetic potential and expression patterns of amino acid and vitamin pathways were  
942 analyzed for the top 15 genomes with the highest transcriptional counts (Table 1). **A)** For  
943 a pathway to be considered present for downstream analysis in the TbasCO pipeline,  
944 80% of the pathway had to be present in a genome. Thus, we used this cutoff criterion to  
945 discern whether a specific pathway was present or absent in a genome (with the  
946 expectation of methionine, as all genomes did not contain at least 80% of the subunits in  
947 the KEGG methionine synthase pathway, we inferred the presence of the methionine  
948 synthase as presence of this pathway). Orange colored boxes for cofactor biosynthesis

949 pathways represents the presence of that pathway, whereas grey infers absence. For  
950 amino acid biosynthetic pathways, amino acids are listed by their side chain groups –  
951 charged, polar, hydrophobic, and other. **B)** Mini-networks of vitamin co-factors. Squares  
952 are genomes with the colors matching the color bar in A. Nodes are attributes, where the  
953 colored nodes for the tetrahydrofolate attributes represent the different routes. **C)** Mini-  
954 networks of amino acid biosynthesis pathways split by type. Colors of nodes for each  
955 amino acid represent the different routes for that pathway. Squares represent genomes  
956 with colors matching the color bar in A.

957  
958 **Table 1.** Genome quality statistics and relative abundance calculations for all 66 EBPR  
959 SBR MAGs. Genome code names match names used in all figures and within the text.  
960 Classifications were assigned using the GTDB-tk [87] and confirmed by comparing  
961 against select publicly available references and a subset of HQ MAGs from Singleton et  
962 al. 2021 [39]. Completeness and redundancy estimates and GC content were calculated  
963 by CheckM [41]. tRNA and rRNA predictions were performed with Barrnap as part of the  
964 Prokka software [88]. Relative abundance estimates reflect the proportion of reads  
965 mapped to the genome in that sample divided by the total number of reads mapped to all  
966 genomes as performed with SingleM. Table available at  
967 [https://figshare.com/articles/dataset/EBPR\\_SBR\\_MAGs\\_Metadata/13063874](https://figshare.com/articles/dataset/EBPR_SBR_MAGs_Metadata/13063874).

968  
969 **Table 2.** KEGG Pathways for core trait-attributes present in greater than 19 genomes.  
970 **Table 3.** KEGG Pathways for differentiating trait-attributes present between 3 and 18  
971 genomes.

972 **Figure 1.**



973

974

975

976

977

978

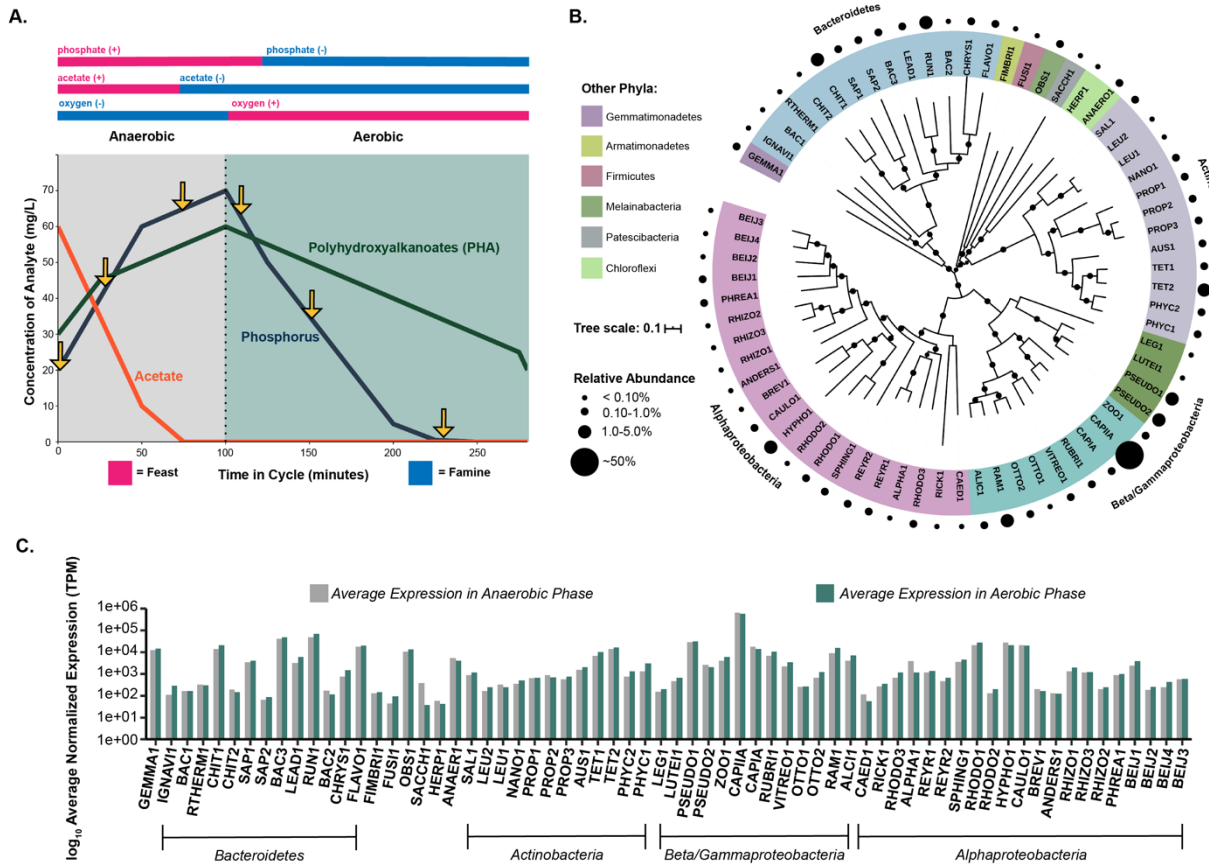
979

980

981

982

983 **Figure 2.**



984

985

986

987

988

989

990

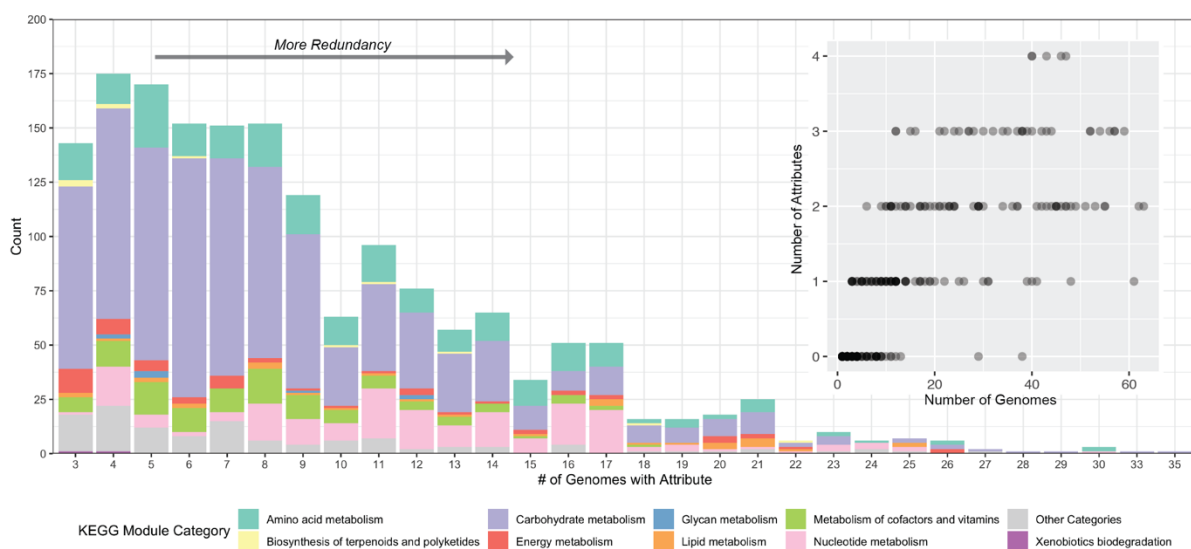
991

992

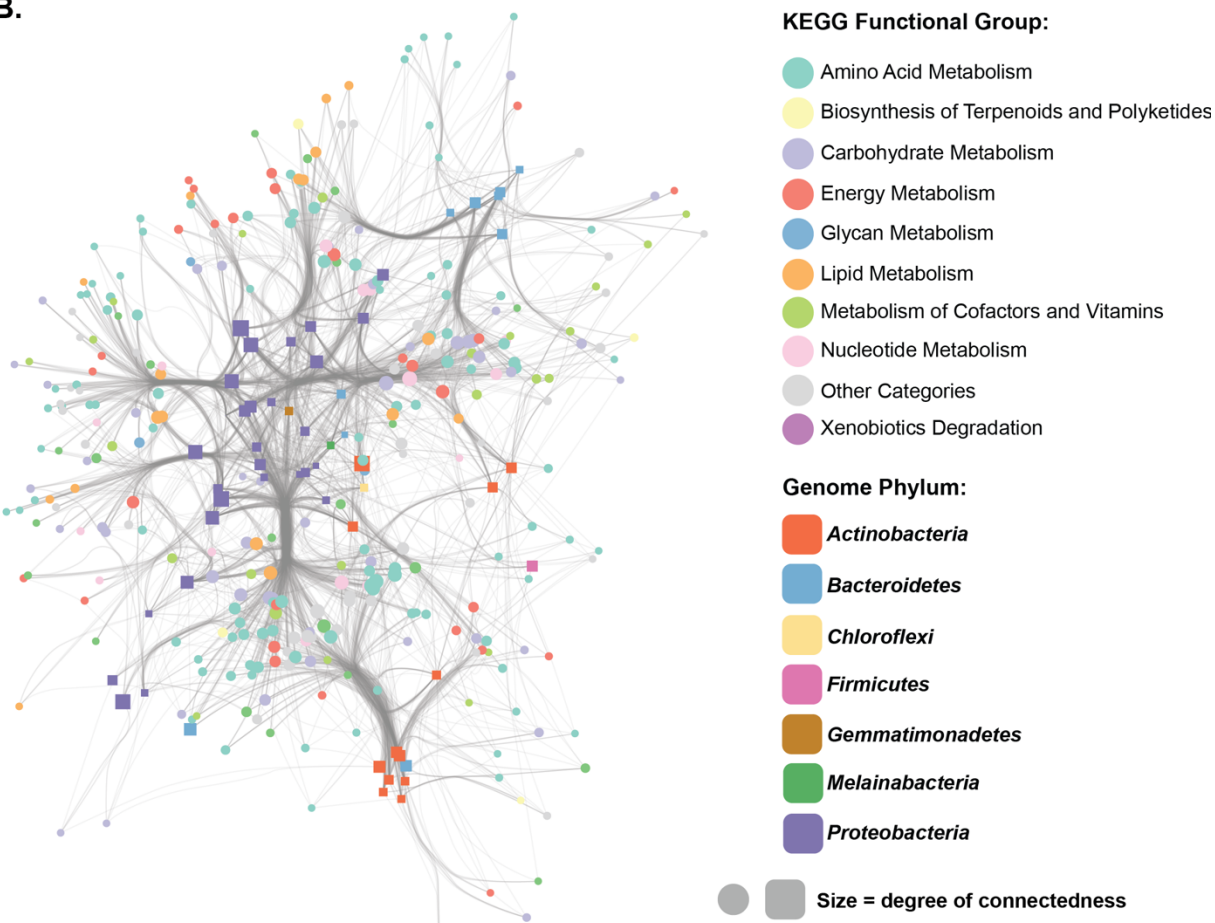
993

994 **Figure 3.**

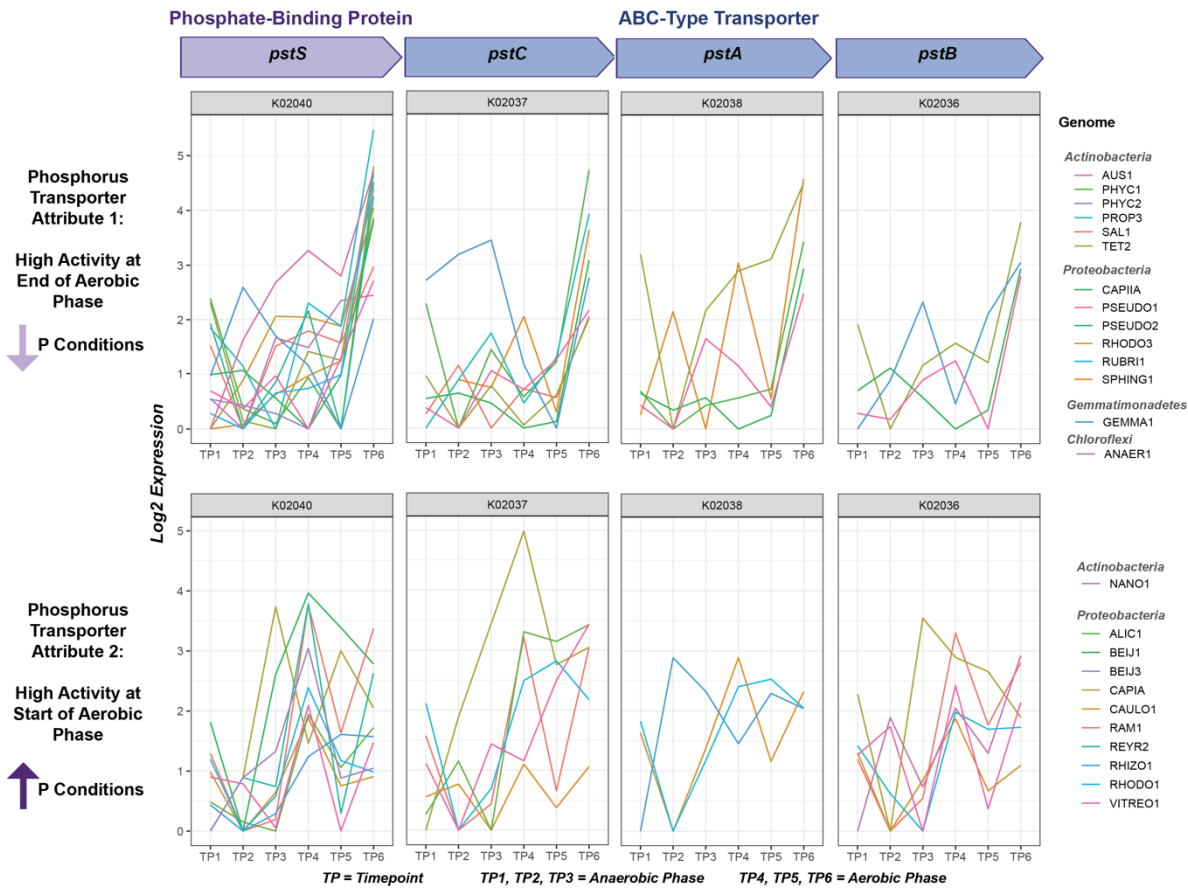
**A.**



**B.**



996 **Figure 4.**



997

998

999

1000

1001

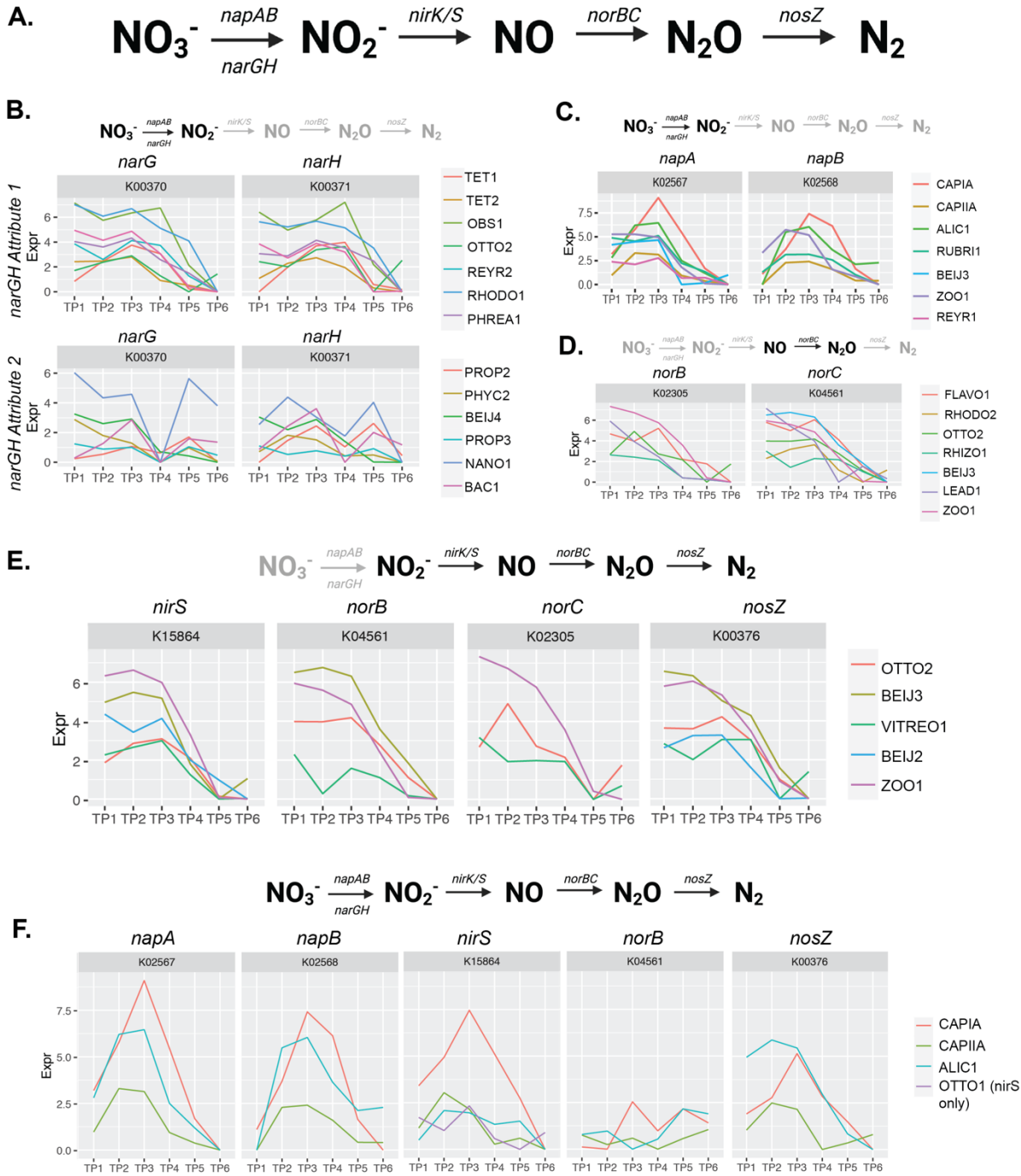
1002

1003

1004

1005

1006 **Figure 5.**

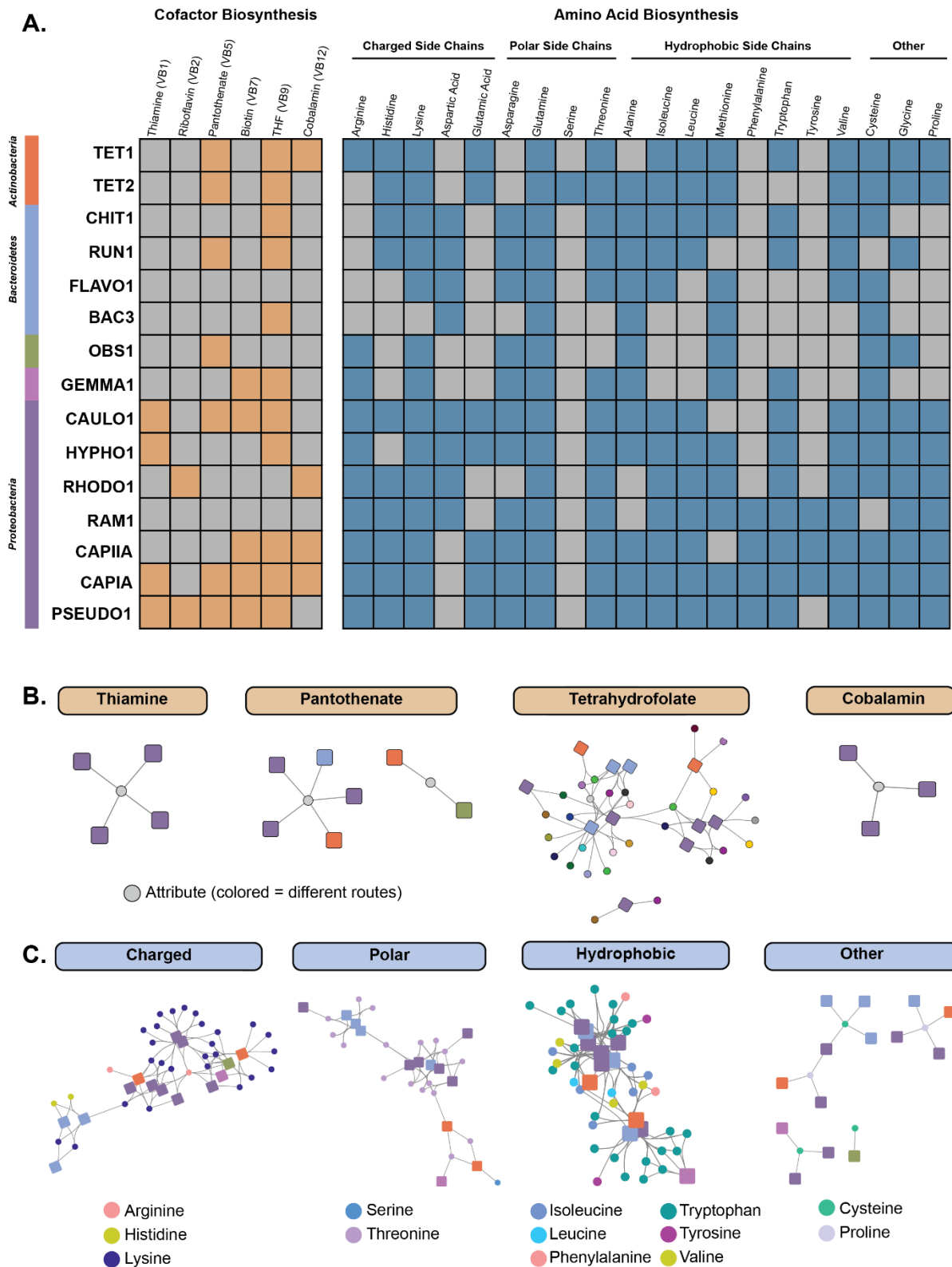


1007

1008

1009

1010 **Figure 6.**



1011 Table 1.

Code	Genbank Accession	Classification	Completeness	Contamination	Size (Mbp)	Configs	GC	Abundance 2013-5-13	Abundance 2013-5-23	Abundance 2013-5-28	Total Transcriptional Reads Mapped	Total rRNAs	Total tRNAs
AUS1	GCA_020161845.1	d_Bacteriop Actinobacteriota Actinobacteriota Actinomycetales f Dermatophilaceae g Austwickiaceae	99.45	5.01	4.39	82	71.2	0.261	0.720	0.124	255331	3	61
PHYC1	GCA_020161851.1	d_Bacteriop Actinobacteriota Actinobacteriota Actinomycetales f Dermatophilaceae g Phycoicoccaceae	98.02	0.54	3.06	34	71	1.355	3.007	0.341	332509	1	49
PHYC2	GCA_020161355.1	d_Bacteriop Actinobacteriota Actinobacteriota Actinomycetales f Dermatophilaceae g Phycoicoccaceae	95.82	1.89	3.20	111	69.2	0.047	0.174	0.112	152031	1	52
TET1	GCA_020160805.1	d_Bacteriop Actinobacteriota Actinobacteriota Actinomycetales f Dermatophilaceae g Tetrasphaera A	98.42	0.54	3.75	57	67.9	0.446	0.436	0.507	1378316	2	47
TEI2	GCA_020160795.1	d_Bacteriop Actinobacteriota Actinobacteriota Actinomycetales f Dermatophilaceae g Tetrasphaera A	98.92	0.05	3.96	66	69.3	0.803	0.236	1.244	2538782	1	76
LEU1	GCA_020161351.1	d_Bacteriop Actinobacteriota Actinobacteriota Actinomycetales f Microbacteriaceae Leucobacters	96.06	2.05	3.01	74	63.5	0.272	0.083	0.093	99061	3	47
LEU2	GCA_020161175.1	d_Bacteriop Actinobacteriota Actinobacteriota Actinomycetales f Microbacteriaceae Leucobacter	83.22	1.48	2.31	140	64.8	0.065	0.101	0.092	22050	2	44
SAL1	GCA_020161051.1	d_Bacteriop Actinobacteriota Actinobacteriota Actinomycetales f Microbacteriaceae Salmibacteriums	97.81	0	2.93	8	67.2	0.335	0.142	0.559	178111	2	45
NAN01	GCA_020161345.1	d_Bacteriop Actinobacteriota Actinobacteriota Actinomycetales f Microbacteriaceae	99.14	3.68	4.29	95	72.7	0.106	0.047	0.172	65510	1	52
PRO1	GCA_020161751.1	d_Bacteriop Actinobacteriota Actinobacteriota Propionibacteriales f Propionibacteriaceae	91.04	0.91	3.47	67	60.3	0.063	0.108	0.046	100351	0	60
PRO2	GCA_020161755.1	d_Bacteriop Actinobacteriota Actinobacteriota Propionibacteriales f Propionibacteriaceae Propionicinomas	93.63	3.02	4.08	61	70.7	0.094	0.046	0.143	130384	3	52
PRO3	GCA_020161015.1	d_Bacteriop Actinobacteriota Actinobacteriota Propionibacteriales f Propionibacteriaceae Propionicinomas	94.14	3.15	3.67	65	71.6	0.074	0.176	0.249	96105	0	51
FMBBII	GCA_020161895.1	d_Bacteriop Actinobacteriota Actinobacteriota Firmicimicodales f Firmimonadaceae Upul-Aris	96.45	0	3.14	38	53.8	0.068	0.224	0.059	297938	3	48
BAC1	GCA_020161835.1	d_Bacteriop Actinobacteriota Actinobacteriota Firmicimicodales f Firmimonadaceae Upul-Aris	94.52	0	4.40	36	41.6	0.345	0.024	0.003	32140	4	42
BAC2	GCA_020162035.1	d_Bacteriop Actinobacteriota Actinobacteriota Firmicimicodales f Firmimonadaceae Upul-Aris	99.05	0.48	3.17	31	29.6	0.757	0.010	0.015	46346	3	32
CHIT1	GCA_020161435.1	d_Bacteriop Bacteroidiota Bacteroidiota AKYH767 f b1-TBQ g x	99.01	0	4.19	10	46.3	0.183	0.174	3.613	3141341	0	34
CHIT2	GCA_020161355.1	d_Bacteriop Bacteroidiota Bacteroidiota Chitinophagales f Chitinophagaceae	100	1.23	4.03	23	48.2	0.195	0.383	0.033	24003	3	40
SAPI	GCA_020160935.1	d_Bacteriop Bacteroidiota Bacteroidiota Chitinophagales f Saprospiraceae	96.53	0.99	5.84	51	50.3	0.226	0.007	0.128	702648	3	36
SAP2	GCA_020160855.1	d_Bacteriop Bacteroidiota Bacteroidiota Chitinophagales f Saprospiraceae OLBBs	97.52	0.5	3.73	65	37.2	0.290	0.167	0.016	10636	3	34
LEAD1	GCA_020161355.1	d_Bacteriop Bacteroidiota Bacteroidiota Cytophagales f Spiromyaceae Leadfetterellae	99.11	0.6	4.81	17	37.7	0.136	0.002	0.858	1017458	2	36
RUN1	GCA_020161055.1	d_Bacteriop Bacteroidiota Bacteroidiota Cytophagales f Spiromyaceae Rimellales Rimellae	100	0	7.44	60	44.4	0.124	1.088	1.749	10275342	2	40
FLAV01	GCA_020161485.1	d_Bacteriop Bacteroidiota Bacteroidiota Flavobacteriales f Flavobacteriaceae Flavobacteriota	99.29	0.35	3.08	18	32.5	0.030	0.002	0.742	302991	3	36
CHRYS1	GCA_020161485.1	d_Bacteriop Bacteroidiota Bacteroidiota Flavobacteriales f Flavobacteriaceae Chryseobacterium A	100	0.25	2.57	11	36.7	0.107	3.917	0.358	209940	2	35
BAC3	GCA_020162015.1	d_Bacteriop Bacteroidiota Bacteroidiota Flavobacteriales f Flavobacteriaceae Chryseobacterium A	100	0	3.74	45	41.1	0.445	0.892	0.693	9991372	0	34
IGNAVII	GCA_020161395.1	d_Bacteriop Bacteroidiota Ignavibacteriales f Ignavibacteriaceae Ag UTCBHB3s	97.27	0.55	4.07	21	42.2	0.163	0.635	0.025	58496	3	44
RTHIERMI	GCA_020160835.1	d_Bacteriop Bacteroidiota Rhodothermio Rhodothermals f g s	98.36	1.38	3.25	36	67	0.328	0.050	0.060	116472	3	52
ANARE1	GCA_020161935.1	d_Bacteriop Chloroflexotac Chloroflexales f Herpetosiphonaceae Herpetosiphons	98.17	0	7.64	32	54.2	0.375	0.190	0.153	910673	4	48
HERP1	GCA_020161265.1	d_Bacteriop Chloroflexotac Chloroflexales f Herpetosiphonaceae Herpetosiphons	99.09	0.91	6.04	13	50.2	0.774	0.025	0.008	7917	0	55
OB51	GCA_020161235.1	d_Bacteriop Cyanobacteriaceae Vampirovibrionicae Obscuribacteriales Obscuribacter	98.28	0.94	5.09	17	49.2	0.672	0.681	0.197	1713299	6	42
FUS11	GCA_020161925.1	d_Bacteriop Firmicutes Aeg Clostridia Peptostreptococcales f Fusibacteriaceae UBA5201s	96.5	1.75	3.08	41	42.8	0.001	0.580	0.001	11649	3	57
GEMMA1	GCA_020161135.1	d_Bacteriop Gemmatimonadotac Gemmatimonadotaceo Gemmatimonadotales	98.35	3.3	4.55	8	70.1	0.004	0.031	0.494	2624259	3	55
SACCH1	GCA_020160975.1	d_Bacteriop Patescibacteriaceae Saccharimonadotac Saccharimonadotales f Saccharimonadotaceae Saccharimonadotus	84.48	0	0.97	1	49.6	0.637	1.437	0.035	65079	3	43
ALPHAI	GCA_020161965.1	d_Bacteriop Proteobacteriaceae Alpha-proteobacteriales f Alpha-proteobacteriaceae	82.43	2.65	3.94	581	64.6	0.015	0.165	0.007	1283274	3	39
CAED1	GCA_020161545.1	d_Bacteriop Proteobacteriaceae Alpha-proteobacteriales f Alpha-proteobacteriaceae	86.36	1.1	1.88	96	52.8	0.034	0.201	0.002	41264	3	35
BREV1	GCA_020161595.1	d_Bacteriop Proteobacteriaceae Alpha-proteobacteriales f Alpha-proteobacteriaceae	97.51	3.41	3.07	155	67.2	0.011	0.254	0.004	27852	2	45
CAUL01	GCA_020161365.1	d_Bacteriop Proteobacteriaceae Alpha-proteobacteriales f Alpha-proteobacteriaceae Caulobacterales	100	0	4.43	25	66.9	0.048	0.093	0.589	462785	3	55
HYPH01	GCA_020161405.1	d_Bacteriop Proteobacteriaceae Alpha-proteobacteriales f Hyphomonomadaceae UBA1942s	98.43	0.32	2.98	6	39.4	0.844	0.006	2.208	4138107	0	33
REYR1	GCA_020160951.1	d_Bacteriop Proteobacteriaceae Alpha-proteobacteriales f Alpha-proteobacteriaceae	89.96	7.34	5.08	210	70	0.057	0.090	0.238	224063	3	53
REYR2	GCA_020160951.1	d_Bacteriop Proteobacteriaceae Alpha-proteobacteriales f Alpha-proteobacteriaceae	91.04	6.01	5.71	258	65.3	0.074	0.102	0.134	62018	1	53
ANDERS1	GCA_020161855.1	d_Bacteriop Proteobacteriaceae Alpha-proteobacteriales f Alpha-proteobacteriaceae	97.64	0.4	3.36	19	61.6	0.187	0.175	0.029	25238	2	46
BE01	GCA_020161751.1	d_Bacteriop Proteobacteriaceae Alpha-proteobacteriales f Alpha-proteobacteriaceae	81.6	8.48	4.44	777	66.3	0.156	0.319	0.423	338238	0	43
BE02	GCA_020161625.1	d_Bacteriop Proteobacteriaceae Alpha-proteobacteriales f Alpha-proteobacteriaceae	81.18	5.25	3.99	465	62.5	0.047	0.157	0.018	28432	0	42
BE03	GCA_020161751.1	d_Bacteriop Proteobacteriaceae Alpha-proteobacteriales f Alpha-proteobacteriaceae	76.21	1.72	3.08	320	63.3	0.007	6.744	0.009	71062	0	41
BE04	GCA_020161751.1	d_Bacteriop Proteobacteriaceae Alpha-proteobacteriales f Alpha-proteobacteriaceae	97.89	0	3.19	17	63.2	0.176	0.538	0.014	26820	0	47
PIRE01	GCA_020161985.1	d_Bacteriop Proteobacteriaceae Alpha-proteobacteriales f Phreatobacteriales Phreatobacteraceae Phreatobacters	98.35	3.96	4.69	38	67.7	0.022	0.273	0.103	132343	1	50
RHIZ01	GCA_020161035.1	d_Bacteriop Proteobacteriaceae Alpha-proteobacteriales f Rhizobiales Rhizobacteriales f Rhizobacteriaceae Aminobacter	94.26	5.5	5.50	89	63.8	0.136	0.095	0.095	219213	3	48
RHIZ02	GCA_020161665.1	d_Bacteriop Proteobacteriaceae Alpha-proteobacteriales f Rhizobiales Rhizobacteriales f Rhizobacteriaceae OFOB01s	88.41	2.12	3.39	43	60.6	0.035	0.325	0.003	24536	0	47
RHIZ03	GCA_020161625.1	d_Bacteriop Proteobacteriaceae Alpha-proteobacteriales f Rhizobiales Rhizobacteriales f Rhizobacteriaceae	78.53	6.03	6.98	935	63.6	0.010	0.169	0.037	149921	0	48
RHOD01	GCA_020161655.1	d_Bacteriop Proteobacteriaceae Alpha-proteobacteriales f Rhodobacteriales f Rhodobacteraceae	100	0.35	4.08	24	65.5	0.321	0.141	0.848	3645270	0	44
RHOD02	GCA_020161615.1	d_Bacteriop Proteobacteriaceae Alpha-proteobacteriales f Rhodobacteriales f Rhodobacteraceae	99.09	1.19	4.87	26	67.9	0.084	0.534	0.009	25807	1	49
RHOD03	GCA_020160875.1	d_Bacteriop Proteobacteriaceae Alpha-proteobacteriales f Rhodospirillales Cf Rhodospirillaceae	91.2	2.27	3.76	236	62.2	0.153	0.046	0.185	153017	1	39
RICK1	GCA_020160775.1	d_Bacteriop Proteobacteriaceae Alpha-proteobacteriales f Ricketsiaceae GCA-2402195s	75.59	1.58	1.18	82	34.5	0.085	0.075	0.052	17671	2	26
SPHIN1	GCA_020160755.1	d_Bacteriop Proteobacteriaceae Alpha-proteobacteriales f Sphingomonadaceae Sphingomonadaceae	99.98	1.56	4.31	20	65.1	0.026	0.014	0.607	606965	3	47
ALIC1	GCA_020161945.1	d_Bacteriop Proteobacteriaceae Gamma-proteobacteriales Burkholderiales f Burkholderiaceae	99.64	1.04	3.83	33	66.3	0.166	2.959	0.738	70970	1	48
OTTO1	GCA_020161715.1	d_Bacteriop Proteobacteriaceae Gamma-proteobacteriales Burkholderiales f Burkholderiaceae	93.66	5.56	4.52	250	67.1	0.011	0.276	0.004	26717	1	46
OTTO2	GCA_020161715.1	d_Bacteriop Proteobacteriaceae Gamma-proteobacteriales Burkholderiales f Burkholderiaceae	99.26	0.62	3.40	35	69.1	0.372	4.140	0.424	121379	1	50
RAM1	GCA_020161775.1	d_Bacteriop Proteobacteriaceae Gamma-proteobacteriales Burkholderiales f Burkholderiaceae	99.84	0.06	4.36	32	66.1	0.778	0.536	1.814	1832037	1	45
RUBRI1	GCA_020161065.1	d_Bacteriop Proteobacteriaceae Gamma-proteobacteriales Burkholderiales f Burkholderiaceae Rubrivivaxs	99.52	0.05	6.29	41	71.2	0.236	0.347	0.306	1259737	1	73
VITRE01	GCA_020161145.1	d_Bacteriop Proteobacteriaceae Gamma-proteobacteriales Burkholderiales f Burkholderiaceae	100	0.7	3.51	13	68.9	0.397	4.498	0.530	382529	1	46
CAPIA	NA	d_Bacteriop Proteobacteriaceae Gamma-proteobacteriales Burkholderiales f Burkholderiaceae	100	0.03	4.59	61	63.8	18.797	10.533	0.106	2411395	0	46
CAPIIA	NA	d_Bacteriop Proteobacteriaceae Gamma-proteobacteriales Burkholderiales f Burkholderiaceae	99.84	0.24	4.64	81	64.3	33.479	26.824	49.334	102762132	0	44
ZOO1	GCA_020161115.1	d_Bacteriop Proteobacteriaceae Gamma-proteobacteriales Burkholderiales f Burkholderiaceae	91.62	3.51	4.99	501	65.7	0.090	0.026	0.106	913411	4	59
LEG1	GCA_020161725.1	d_Bacteriop Proteobacteriaceae Gamma-proteobacteriota Legionellales f Legionellaceae	92.74	1.07	2.58	182	36.1	0.094	0.126	0.006	19591	1	27
LUET1	GCA_020161335.1	d_Bacteriop Proteobacteriaceae Gamma-proteobacteriota Xanthomonadales f Xanthomonadaceae Luteimonas	96.89	0.71	3.56	252	69.9	0.002	0.309	0.011	49418	1	39
PSEUDO1	GCA_020160895.1	d_Bacteriop Proteobacteriaceae Gamma-proteobacteriota Xanthomonadales f Xanthomonadaceae Pseudoxanthomonas A	99.95	0.89	3.67	28	67.8	0.016	0.730	3.125	3964795	2	50
PSEUDO2	GCA_020161075.1	d_Bacteriop Proteobacteriaceae Gamma-proteobacteriota Xanthomonadales f Xanthomonadaceae Pseudoxanthomonas	99.02	0	2.99	6	69.6	1.750	6.111	1.228	515369	3	52

1012

1013

File at <https://figshare.com/account/projects/90437/articles/13063874>

1014

1019  
1020**Table 2.**

Module Description	Number of Attributes
Citrate cycle, second carbon oxidation, 2-oxoglutarate => oxaloacetate [PATH:map00020 map01200 map01100]	13
Citrate cycle (TCA cycle, Krebs cycle) [PATH:map00020 map01200 map01100]	10
Shikimate pathway, phosphoenolpyruvate + erythrose-4P => chorismate [PATH:map00400 map01230 map01100 map01110]	8
Fatty acid biosynthesis, initiation [PATH:map00061 map01212 map01100]	7
Glycolysis, core module involving three-carbon compounds [PATH:map00010 map01200 map01230 map01100]	7
Adenine ribonucleotide biosynthesis, IMP => ADP,ATP [PATH:map00230 map01100]	4
Guanine ribonucleotide biosynthesis IMP => GDP,GTP [PATH:map00230 map01100]	4
Inosine monophosphate biosynthesis, PRPP + glutamine => IMP [PATH:map00230 map01100]	4
Isoleucine biosynthesis, threonine => 2-oxobutanoate => isoleucine [PATH:map00290 map01230 map01100]	3
NADH:quinone oxidoreductase, prokaryotes [PATH:map00190]	3
beta-Oxidation, acyl-CoA synthesis [PATH:map00061 map00071 map01212 map01100]	2
F-type ATPase, prokaryotes and chloroplasts [PATH:map00190 map00195]	2
Valine/isoleucine biosynthesis, pyruvate => valine / 2-oxobutanoate => isoleucine [PATH:map00290 map00770 map01210 map01230 map01100 map01110]	2
CAM (Crassulacean acid metabolism), dark [PATH:map00620 map00710 map01200 map01100 map01120]	1
Cytochrome c oxidase, cbb3-type [PATH:map00190]	1
Cytochrome c oxidase, prokaryotes [PATH:map00190]	1
dTDP-L-rhamnose biosynthesis [PATH:map00521 map00523 map01100 map01130]	1
Leucine biosynthesis, 2-oxoisovalerate => 2-oxoisocaproate [PATH:map00290 map01210 map01230 map01100 map01110]	1
Phosphatidylethanolamine (PE) biosynthesis, PA => PS => PE [PATH:map00564 map01100]	1
PRPP biosynthesis, ribose 5P => PRPP [PATH:map00030 map00230 map01200 map01230 map01100]	1
Pyruvate oxidation, pyruvate => acetyl-CoA [PATH:map00010 map00020 map00620 map01200 map01100]	1
Semi-phosphorylative Entner-Doudoroff pathway, gluconate => glycerate-3P [PATH:map00030 map01200 map01100 map01120]	1
Threonine biosynthesis, aspartate => homoserine => threonine [PATH:map00260 map01230 map01100 map01110]	1

1021

1022  
1023**Table 3.**

Module_description	Number of Attributes
Glycolysis (Embden-Meyerhof pathway), glucose => pyruvate [PATH:map00010 map01200 map01100]	279
Citrate cycle (TCA cycle, Krebs cycle) [PATH:map00020 map01200 map01100]	208
Gluconeogenesis, oxaloacetate => fructose-6P [PATH:map00010 map00020 map01100]	76
Inosine monophosphate biosynthesis, PRPP + glutamine => IMP [PATH:map00230 map01100]	45
Citrate cycle, second carbon oxidation, 2-oxoglutarate => oxaloacetate [PATH:map00020 map01200 map01100]	31
Heme biosynthesis, plants and bacteria, glutamate => heme [PATH:map00860 map01100 map01110]	27
Tetrahydrofolate biosynthesis, GTP => THF [PATH:map00790 map00670 map01100]	25
Tryptophan biosynthesis, chorismate => tryptophan [PATH:map00400 map01230 map01100 map01110]	25
Ornithine biosynthesis, glutamate => ornithine [PATH:map00220 map01210 map01230 map01100]	24
Histidine biosynthesis, PRPP => histidine [PATH:map00340 map01230 map01100 map01110]	17
Pentose phosphate pathway (Pentose phosphate cycle) [PATH:map00030 map01200 map01100 map01120]	16
Lysine biosynthesis, succinyl-DAP pathway, aspartate => lysine [PATH:map00300 map01230 map01100]	12
Uridine monophosphate biosynthesis, glutamine (+ PRPP) => UMP [PATH:map00240 map01100]	11

1024